# Computing the dynamics of biomembranes by combining conservative level set and adaptive finite element methods

Aymen Laadhari, Pierre Saramito, Chaouqi Misbah

# Computing the dynamics of biomembranes by combining conservative level set and adaptive finite element methods

Aymen Laadhari[a], Pierre Saramito[a,*], Chaouqi Misbah[b]

[a] *Lab. Jean Kuntzmann, Université Joseph Fourier and CNRS, F-38041 Grenoble France*

[b] *Lab. Interdisciplinaire de Physique, Université Joseph Fourier and CNRS, F-38041 Grenoble France*

**Abstract**

The numerical simulation of the deformation of vesicle membranes under simple shear external fluid flow is considered in this paper. A new saddle-point approach is proposed for the imposition of the fluid incompressibility and the membrane inextensibility constraints, through Lagrange multipliers defined in the fluid and on the membrane respectively. Using a level set formulation, the problem is approximated by mixed finite elements combined with an automatic adaptive mesh procedure at the vicinity of the membrane boundary. Numerical experiments show that this combination of the saddle-point and adaptive mesh method enhances the robustness of the method. The effect of inertia on the stability of the vesicle is also investigated.

*Keywords:* level set method, mass conservation, adaptive finite element method, Helfrich energy, vesicle dynamics, red cell membrane, simple shear flow

## 1. Introduction

Phospholipid membranes are abundant in biology. They represent the major component of the cytoplasmic membrane of real cells. They are also present within the cell cytoplasm, e.g. the Golgi apparatus, a complex assembly of phospholipid layers which serve to form small vesicles for protein transport. Phospholipid membranes are also used in many industrial applications, as in giant liposome emulsions for cosmetics. A simple closed membrane of pure phospholipid suspended in an aqueous solution, also called a suspension of *vesicles*, constitute an attractive model system in order to describe mechanical and viscoelastic behaviors of many cells, like red blood cells. They are also considered as promising drug carriers for a delivery at specific sites in the organisms. This explains the increasing interest for biological membranes from various communities ranging from biology [38, 34] to applied mathematics [36, 21, 4]. This contribution is concerned with a certain aspect of mathematical modeling of vesicles, and more generally of phospholipid membranes.

Vesicles are formed by amphiphilic molecules self-assembled in water to build bilayers, in a certain range of concentration and temperature. At room, as well as at the physiological temperature, the membrane is a two dimensional incompressible fluid. Due to incompressibility, the main mode of deformation of a vesicle is bending. A basic ingredient for biomembranes is thus bending energy. Canham [9] and

*Corresponding author

*Email addresses:* Aymen.Laadhari@imag.fr (Aymen Laadhari), Pierre.Saramito@imag.fr (Pierre Saramito), cmisbah@ujf-grenoble.fr (Chaouqi Misbah)

Helfrich [18, 30] introduced the following expression of the bending energy:

$$\frac{k}{2}\int_\Gamma (H-H_0)^2\,\mathrm{d}s + \frac{k_g}{2}\int_\Gamma K\,\mathrm{d}s, \tag{1}$$

where $H = H_1 + H_2$ is the mean curvature of the membrane surface, with $H_1$ and $H_2$ are the principle curvatures and $K = H_1H_2$ is the Gauss curvature. The membrane surface is denoted by $\Gamma$ while $\Omega$ represents the volume inside the vesicle, such that $\Gamma = \partial\Omega$. The integrals are performed along the membrane surface where $\mathrm{d}s$ denotes a surface area, while, in this paper, $\mathrm{d}x$ will represent a volume element. The constants $k$ and $k_g$ have the dimension of an energy and represent the bending modulus and the Gaussian curvature modulus, respectively. Also $H_0$ denotes the spontaneous curvature that describes the asymmetry of the membrane. In this paper, $H_0 = 0$, since $H_0$ is relevant only for three-dimensional problems (see appendix Appendix A) and we restrict to the bidimensional case in this paper. Finally, from the Gauss-Bonnet theorem, the second term of the Canham-Helfrich energy (1) is a topological invariant. Since topological changes are not considered in this paper, this second term is omitted here.

Vesicles can be more or less inflated. The deflation could be due to osmotic effects, depending on additives in the solution. It could also be due to thermal effects: the thermal expansion of phospholipids is greater than those of the water inside the membrane, and thus, the area $A_0$ of the vesicle increases more rapidly than its volume $V_0$. The *reduced volume*, denoted as $\gamma$, measures the deflation:

$$\gamma = \frac{3V_0}{4\pi}\times\left(\frac{4\pi}{A_0}\right)^{3/2} \in\, ]0,1]. \tag{2}$$

Thus, $\gamma$ compares the vesicle volume $V_0$ with the volume of a sphere having the area equal to $A_0$: $\gamma$ is a number without dimension, that equals to 1 when the vesicle is a sphere and is lower than 1 otherwise. For instance, for the human red blood cell $\gamma \approx 0.64$. By varying $\gamma$, the shape that minimizes the energy of curvature can vary from an ellipsoid stretched to a biconcave shape, towards forms varied as that of the Peanut. In the two-dimensional case, $V_0$ and $A_0$ denotes the area and the perimeter respectively. The reduced area $\gamma$ compares the area of the vesicle with the area of a circle having the same perimeter as the vesicle. The reduced area is expressed in the two-dimensional case by:

$$\gamma \;=\; \frac{V_0}{\pi}\times\left(\frac{2\pi}{A_0}\right)^2.$$

Notice that, for a circle, the reduced area equals to 1.

Notice that the vesicle membrane is impermeable (no osmosis), the number of molecules remains fixed in each layer, and the energetic cost of stretching or compressing the membrane is much larger than the cost of bending deformations: the membrane could be considered as inextensible. In order to satisfy this inextensibility constraint, two approaches are commonly available. The first one use the penalty approach, together with a penalty parameter (see e.g. [10, 12]): the inextensibility constraint then is not exactly satisfied and the approximate solution depends upon the penalty parameter. The second solution introduces a Lagrange multiplier, that interprets as the surface tension of the membrane, and the inextensibility constraints is exactly satisfied. In our present work, the second solution was selected, since it avoid the dependence of the solution upon the penalty parameter. Despite it has not yet retain attentions in the context of membrane vesicle application, it is of common use for incompressible fluid flow applications (see e.g. [35]).

Furthermore, for general interface fluid flow problems, there are two main classes of numerical methods usually used: the Lagrangian methods class based on an explicit interface parameterization and discretization while the Eulerian methods class uses an implicit function that expresses the interface by its equation. The popular phase field and level set methods fall into this second class.

For Lagrangian methods, the interface, which represents here the biological membrane, is discretized by a set of points which are going to be moved with a speed depending on the studied problem. The mesh, capturing the interface, may regenerated at each time step, while the boundary conditions between inside and outside volume of the interface could be directly imposed at the element level. The older method used for vesicle fluid application falls into this category: the *boundary element method* transforms all viscous volume terms into surface integrals through a Green kernel and only a surface mesh of the interface is required [32, 33]. Nevertheless, inertia terms are not reducible to boundary integrals and, despite some recent improvements, this approach suffers from some limitations. A more recent approach bases on both a mesh of the interface and a volume mesh. When the volume mesh is compatible with the interface discretization, the *classical finite element method* could be used [8]. A commonly used variant fixes the volume mesh one time for all and expresses interface integrals on a discrete moving surface mesh: this is the so called *penalty immersed boundary method* [23, 24].

The Eulerian methods are characterized by the use of a meshing strategy that is independent of the movements of the interface: this approach allows the use of fixed and fully structured volume mesh. Moreover, no more surface mesh of the moving interface is required. Very complex shapes, with strong variations of the curvature and possible topological changes, becomes also possible. In the case of a diffuse interface, as for fluid mixtures, the interface is represented by a smooth transition zone. Indeed, at least at the molecular scale, there is a small zone of mixture between species. From a numerical point of view, the diffuse interface notion could be interpreted as a way of regularization of a sharp model interface, together with a regularization parameter, associated to the interface width: this is the *phase field method*, introduced by Allen and Cahn [2], and applied recently to vesicles [5, 11]. A second Eulerian method, the *level set method* [29], do no more requires any regularization and is able to catch sharp interfaces: a simple transport equation is used to move the level set function. See [28] for applications to vesicle dynamics.

Nevertheless, both phase field and level set methods suffer a lack of precision when dealing with the inextensibility constraints. In this paper we develop a new level set method that exactly solve these constraints at the discrete level: it extends to the vesicle dynamics a previous work on level set methods for the advection equation [26].

In the present work we focus our attention on describing the dynamics of a single suspended vesicle in a linear shear gradient of a plane flow. Vesicles in shear flow in the limit of the vanishing Reynolds number (also called the Stokes limit) have been the subject of extensive studies [4]. In the present work, inertia terms are not neglected, and non-zero Reynolds numbers are considered. This situation is more realistic for both red blood cells and vesicle practical flows applications.

An outline of the paper is as follows. A saddle-point approach allows us to characterize the solution in a weak formulation, which is discretized using mixed finite elements in section 2. In Section 3 we focus on the numerical method. We present our level set method formulation for the vesicle dynamics and show the finite element discretization as well the advection mass preservation improvement. Section

4 is devoted to show numerical results illustrating the vesicle membrane in the tumbling and the tank-treading regimes. Finally, for the first time, the effect of the inertia terms is elaborated and we show that beyond a critical value of the number of Reynolds the vesicle passes from a tumbling to a tank-treading regime.

## 2. Problem statement

### *2.1. Notations and preliminary results*

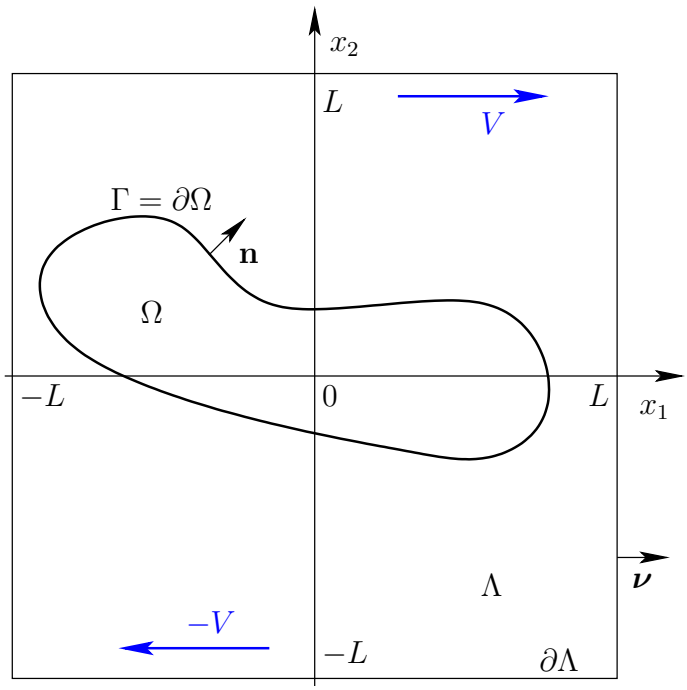


Figure 1: Notations for the vesicle interacting with a surrounding shear flow.

Let $\Lambda = ]-L, L[^d$ be the bounded region containing the vesicle and the surrounding fluid, where $L > 0$ is the half domain width. Numerical computations are performed in this paper with $d = 2$, while the mathematical formulation could be extended to $d = 3$ with few modifications. Let $T > 0$: for any $t \in ]0, T[$, the membrane $\Gamma(t) \subset \Lambda$ is the closed surface defined by:

$$\Gamma(t) = \{(t, x) \in ]0, T[\times\Lambda; \quad \phi(t, x) = 0\}, \tag{3}$$

where $\phi$ is the level set function. By convention, the vesicle $\Omega(t) \subset \Lambda$ is the region where $\phi(t, .)$ is negative and we have $\Gamma(t) = \partial\Omega(t)$.

Let $\mathbf{u}$ denotes the velocity of the fluid in $\Lambda$. The membrane $\Gamma(t)$ is transported at the same velocity, and thus, the level set function satisfies:

$$\frac{D\phi}{Dt} = \frac{\partial\phi}{\partial t} + \mathbf{u}.\nabla\phi = 0 \quad \text{in} \quad ]0, T[\times\Lambda, \tag{4a}$$

where $D/Dt$ denotes the material derivative. The previous transport equation may be completed by suitable boundary and initial conditions:

$$\phi = \phi_b \quad \text{on} \quad ]0, T[\times\Sigma_- \tag{4b}$$

$$\phi(0) = \phi_0 \quad \text{in} \quad \Lambda \tag{4c}$$

where $\Sigma_- = \{x \in \partial\Lambda;\ \mathbf{u}.\boldsymbol{\nu}(x) < 0\}$ is the upstream and $\boldsymbol{\nu}$ denotes the outward unit normal to the surrounding bounding box $\Lambda$. Concerning the initial condition (4c), the function $\phi_0$ denotes the *signed distance* between $x$ and the given initial shape membrane $\partial\Omega(0)$:

$$\phi_0(x) = \begin{cases} \inf\{|y-x|;\ y \in \partial\Omega(0)\} & \text{when } x \notin \Omega(0), \\ \inf\{-|y-x|;\ y \in \partial\Omega(0)\} & \text{otherwise.} \end{cases}$$

Let $\mathbf{n}$ denotes the unit outward normal vector to the shape $\Omega$ (see Fig. 1). Let $f$ be any scalar function and $\mathbf{v}$ be any vector field. The surface gradient, the surface divergence and the Laplace-Beltrami operator are respectively expressed by:

$$\nabla_s f = (I - \mathbf{n}\otimes\mathbf{n})\,\nabla f = \nabla f - (\mathbf{n}.\nabla f)\,\mathbf{n}, \tag{5a}$$

$$\mathrm{div}_s\,\mathbf{v} = (I - \mathbf{n}\otimes\mathbf{n}) : \nabla\mathbf{v} = \mathrm{div}\,\mathbf{v} - ((\nabla\mathbf{v}).\mathbf{n}).\mathbf{n}, \tag{5b}$$

$$\Delta_s f = \mathrm{div}_s\,(\nabla_s f)\,. \tag{5c}$$

Here, $\otimes$ denotes the tensorial product of two vectors and the semicolumn : is the two times contracted product between tensors.

The mean and the Gauss curvatures can be expressed in terms of the normal $\mathbf{n}$ (see [25]):

$$\begin{aligned} H &= \nabla_s.\mathbf{n} = \nabla.\mathbf{n}, \\ 2K &= H^2 - \nabla\mathbf{n} : \nabla\mathbf{n}^T. \end{aligned}$$

### *2.2. Minimization and saddle-point formulations*

For any velocity field $\mathbf{u}$ defined in $]0,T[\times\Lambda$, the instantaneous energy of the system is defined at any time $t \in ]0,T[$ by:

$$J(\mathbf{u}(t)) = \int_\Lambda \eta\,|D(\mathbf{u}(t))|^2\,\mathrm{d}x + \int_{\partial\Omega(t)} \frac{k}{2}H^2\,\mathrm{d}s, \tag{6}$$

where $D(\mathbf{u}) = (\nabla\mathbf{u} + (\nabla\mathbf{u})^T)/2$ is the symmetric part of the gradient of velocity tensor and $|.|$ denotes the Euclidean norms of vectors or tensors. The previous expression of the energy includes two terms: the viscous energy and the Canham-Helfrich bending energy. There are two corresponding scalar parameters: $\eta$ is the viscosity and $k$ the bending modulus of the Canham-Helfrich energy introduced in (1). In practice, the viscosity $\eta$ is not constant over $\Lambda$: it takes a constant value $\eta_0$ outside the vesicle $\Omega(t)$ and a different constant value $\eta_1$ inside the vesicle.

Notice that, in the bending energy term in (6), the membrane $\partial\Omega(t)$ depends upon the velocity field $\mathbf{u}$ via (3) and the level-set function $\phi$, satisfying the transport problem (4) that involves $\mathbf{u}$. Also, the curvature $H$ on $\partial\Omega(t)$ depends implicitly upon $\mathbf{u}$.

The unknown velocity field may satisfy the boundary conditions and two additional constraints: the fluid mass conservation and the membrane inextensibility. The mass conservation reduces to the divergence-free condition $\mathrm{div}\,\mathbf{u} = 0$ since the density, denoted by $\rho$, is supposed to be constant. Conversely, the membrane inextensibility writes locally $\mathrm{div}_s\,\mathbf{u} = 0$. Let us introduce the following spaces of admissible velocities:

$$\begin{aligned} \mathbb{V}(\mathbf{u}_b) &= \left\{\mathbf{v} \in \left(H^1(\Lambda)\right)^d;\ \mathbf{v} = \mathbf{u}_b \ \text{ on } \Sigma_D\right\}, \\ \mathbb{K}(t,\mathbf{u}_b) &= \{\mathbf{v} \in \mathbb{V}(\mathbf{u}_b);\ \mathrm{div}\,\mathbf{v} = 0 \text{ in } \Lambda \text{ and } \mathrm{div}_s\,\mathbf{v} = 0 \text{ on } \partial\Omega(t)\}\,. \end{aligned}$$

The boundary $\Sigma_D = ]-L, L[^{d-1} \times \{-L, L\}$ is associated to the Dirichlet boundary condition $\mathbf{u}_b(t,x)$, expressed for a shear flow by:

$$\mathbf{u}_b(t,x) = \begin{cases} V & \text{when } x_d = L \\ -V & \text{when } x_d = -L \end{cases}$$

for all $(t,x) \in ]0,T[ \times \Sigma_D$. Here, $V$ denotes the given shear velocity at the surrounding box boundary (see Fig. 1). Finally, the problem expresses as a minimization one:

*find* $\mathbf{u} \in C^0\left(]0,T[, L^2(\Lambda)^d\right) \cap L^2\left(]0,T[, \mathbb{K}(t,\mathbf{u}_b)\right)$ *such that*

$$\begin{cases} \mathbf{u}(t) &= \underset{\mathbf{v} \in \mathbb{K}(t,\mathbf{u}_b)}{\arg\inf}\, J(\mathbf{v}), \ \forall t \in ]0,T[, \\ \\ \mathbf{u}(0) &= \mathbf{u}_0 \ \text{ in } \ \Lambda. \end{cases}$$

where $\mathbf{u}_0$ is the given initial velocity. This is a strongly nonlinear shape optimization problem, expressed in terms of the unknown $\mathbf{u}$.

The space of admissible velocities $\mathbb{K}(t,\mathbf{u}_b)$ contains the incompressibility and inextensibility constraints: it is not suitable for practical finite element discretization, since there are no known finite element basis of such spaces. Conversely, the unconstrained space of $\mathbb{V}(\mathbf{u}_b)$ is of practical interest: the two constraints can be imposed via two Lagrange multipliers: the pressure $p$ and the surface tension $\lambda$. Let us introduce the following Lagrangian:

$$\mathscr{L}(\mathbf{u};\, p, \lambda) = J(\mathbf{u}) + \int_\Lambda p \operatorname{div} \mathbf{u} \, \mathrm{d}x + \int_{\partial\Omega(t)} \lambda \operatorname{div}_s \mathbf{v} \, \mathrm{d}s.$$

The previous minimization problem can be rewritten as a saddle point problem:

*find* $\mathbf{u} \in C^0\left(]0,T[, L^2(\Lambda)^d\right) \cap L^2\left(]0,T[, \mathbb{V}(\mathbf{u}_b)\right)$, $p \in L^2\left(]0,T[, L^2(\Lambda)\right)$
*and* $\lambda \in L^2\left(]0,T[, H^{\frac{1}{2}}(\Lambda)\right)$ *such that*

$$\begin{cases} (\mathbf{u}, p, \lambda) &= \underset{\mathbf{v} \in \mathbb{V}(\mathbf{u}_b)}{\arg\inf} \ \underset{\substack{q \in L^2(\Lambda) \\ \mu \in H^{\frac{1}{2}}(\partial\Omega(t))}}{\sup} \ \mathscr{L}(\mathbf{v};\, q, \mu), \\ \\ \mathbf{u}(0) &= \mathbf{u}_0 \ \text{ in } \ \Lambda. \end{cases}$$

Here $H^{\frac{1}{2}}(\partial\Omega)$ denotes as usual [1] the space of the trace of elements of $H^1(\Omega)$ on $\partial\Omega$.

### *2.3. Variational formulation*

Since the Lagrangian $\mathscr{L}$ is differentiable, the saddle point $(\mathbf{u}; p, \lambda)$ satisfies the following variational optimality system:

$$\begin{aligned} \frac{\partial \mathscr{L}}{\partial \mathbf{u}}(\mathbf{u};\, p, \lambda)(\mathbf{v}) &= 0, \quad \forall \mathbf{v} \in \mathbb{V}(0), \\ \frac{\partial \mathscr{L}}{\partial p}(\mathbf{u};\, p, \lambda)(q) &= 0, \quad \forall q \in L^2(\Lambda), \\ \frac{\partial \mathscr{L}}{\partial \lambda}(\mathbf{u};\, p, \lambda)(\mu) &= 0, \quad \forall \mu \in H^{\frac{1}{2}}(\partial\Omega). \end{aligned}$$

Remark that, since $J$ is not convex in general, the previous optimality system could include both local minimums and maximums of the energy $J$. Thus, this

optimality system is not equivalent to the minimization or saddle-point problems; nevertheless, a minimum of $J$ is also a solution of the optimality system. After expansion of the derivatives of $\mathscr{L}$, the optimality system leads to the following variational formulation of the problem:

*find* $\mathbf{u} \in C^0\left(]0,T[, L^2(\Lambda)^d\right) \cap L^2\left(]0,T[, \mathbb{V}(\mathbf{u}_b)\right)$, $p \in L^2\left(]0,T[, L^2_0(\Omega)\right)$ *and* $\lambda \in L^2\left(]0,T[, H^{\frac{1}{2}}(\partial\Omega)\right)$ *such that*

$$\begin{aligned}
\int_\Lambda \rho \frac{D\mathbf{u}}{Dt}.\mathbf{v}\,\mathrm{d}x + \int_\Lambda 2\eta\, D(\mathbf{u}) : D(\mathbf{v})\,\mathrm{d}x & \\
+ \int_\Lambda p\ \mathrm{div}\,\mathbf{v}\,\mathrm{d}x + \int_{\partial\Omega(t)} \lambda\, \mathrm{div}_s\,\mathbf{v}\,\mathrm{d}s &= \int_{\partial\Omega(t)} \mathbf{f}.\mathbf{v}\,\mathrm{d}s, \quad \forall \mathbf{v} \in \mathbb{V}(0), \qquad (7a)\\
\int_\Lambda q\ \mathrm{div}\,\mathbf{u}\,\mathrm{d}x &= 0, \quad \forall q \in L^2(\Lambda), \qquad (7b)\\
\int_{\partial\Omega(t)} \mu\, \mathrm{div}_s\,.\mathbf{u}\,\mathrm{d}s &= 0, \quad \forall \mu \in H^{\frac{1}{2}}(\partial\Omega(t)). \qquad (7c)
\end{aligned}$$

together with the initial condition $\mathbf{u}(0) = \mathbf{u}_0$. Recall that $\partial\Omega(t)$ is given by (3) in terms of the level set function $\phi$, which is solution of the transport problem (4a)-(4c) involving $\mathbf{u}$. We have introduced the material time derivative $\dfrac{D\mathbf{u}}{Dt} = \partial_t\mathbf{u} + \mathbf{u}.\nabla\mathbf{u}$: it expresses the velocity time derivative in the (fixed) Eulerian frame and involves the nonlinear inertia term. The strength $\mathbf{f}$, that appears in the right-hand-side of (7a), is associated to the Canham-Helfrich bending energy and is given by [30, 25]:

$$\mathbf{f} = k\left\{\Delta_s H + H\left(\frac{H^2}{2} - 2K\right)\right\}\mathbf{n}.$$

This is not an obvious computation, since $\partial\Omega(t)$ and $H$ depend implicitly upon $\mathbf{u}$: it requires some advanced shape optimization tools. In the two-dimensional case, since $K = 0$, this expression reduces to: $\mathbf{f} = k\left(\Delta_s H + H^3/2\right)\mathbf{n}$.

### *2.4. Strong formulation*

In order to deal with the integrals over $\partial\Omega(t)$, a generalization of the Green formula over the closed surface $\partial\Omega(t)$ is used (see e.g. [25]):

$$\int_{\partial\Omega} \nabla_s\mu.\mathbf{v}\,\mathrm{d}s + \int_{\partial\Omega} \mu\,\mathrm{div}_s\,\mathbf{v}\,\mathrm{d}s = \int_{\partial\Omega} \mu\,\mathbf{v}.\mathbf{n}\,H\,\mathrm{d}s, \quad \forall \mu \in H^{\frac{1}{2}}(\partial\Omega), \quad \forall \mathbf{v} \in H^1(\Lambda). \qquad (8)$$

Equation (7a) is then integrated by parts on $\Omega$ and $\Lambda\backslash\overline{\Omega}$ and terms are then merged. Thus, for all $\mathbf{v} \in \mathbb{V}(0)$, we have:

$$\begin{aligned}
\int_\Lambda \rho \frac{D\mathbf{u}}{Dt}.\mathbf{v}\,\mathrm{d}x - \int_\Lambda \mathbf{div}\left(2\eta\, D(\mathbf{u}) - pI\right).\mathbf{v}\,\mathrm{d}x + \int_{\partial\Lambda} \left\{\left(2\eta\, D(\mathbf{u}) - pI\right).\boldsymbol{\nu}\right\}.\mathbf{v}\,\mathrm{d}s & \\
+ \int_{\partial\Omega(t)} \left\{\left[2\eta\, D(\mathbf{u}) - pI\right].\mathbf{n}\right\}.\mathbf{v}\,\mathrm{d}s - \int_{\partial\Omega(t)} \nabla_s\lambda.\mathbf{v}\,\mathrm{d}s + \int_{\partial\Omega(t)} \lambda\, H\mathbf{n}.\mathbf{v}\ \mathrm{d}s & \\
= \int_{\partial\Omega(t)} \mathbf{f}.\mathbf{v}\,\mathrm{d}s &
\end{aligned}$$

where [.] denotes the jump of a quantity across $\partial\Omega(t)$ in the direction $\mathbf{n}$ of the normal, $I$ is the identity tensor and **div** is the divergence of a symmetric tensor, defined as the divergence of its row or column vectors.

Finally, the strong form of the problem writes:

*find* $\phi$, $\mathbf{u}$, $p$ *and* $\lambda$ *such that*

$$\begin{aligned}
\frac{\partial \phi}{\partial t} + \mathbf{u}.\nabla\phi &= 0 \ \text{ in } ]0,T[\times\Lambda && \text{(9a)}\\
\rho\left(\frac{\partial \mathbf{u}}{\partial t} + \mathbf{u}.\nabla\mathbf{u}\right) - \mathbf{div}\left(2\eta\, D(\mathbf{u})\right) + \nabla p &= 0 \ \text{ in } ]0,T[\times(\Lambda\backslash\partial\Omega) && \text{(9b)}\\
\operatorname{div}\mathbf{u} &= 0 \ \text{ in } ]0,T[\times\Lambda && \text{(9c)}\\
[\mathbf{u}] &= 0 \ \text{ on } ]0,T[\times\partial\Omega && \text{(9d)}\\
-k\left\{\Delta_s H + H\left(\frac{H^2}{2} - 2K\right)\right\}\mathbf{n} & \\
+H\,\lambda\,\mathbf{n} - \nabla_s\lambda + \left[2\eta\, D(\mathbf{u}) - pI\right].\mathbf{n} &= 0 \ \text{ on } ]0,T[\times\partial\Omega && \text{(9e)}\\
\operatorname{div}_s\mathbf{u} &= 0 \ \text{ on } ]0,T[\times\partial\Omega && \text{(9f)}\\
\phi &= \phi_b \ \text{ on } ]0,T[\times\Sigma_- && \text{(9g)}\\
\mathbf{u} &= \mathbf{u}_b \ \text{ on } ]0,T[\times\Sigma_D && \text{(9h)}\\
(2\eta D(\mathbf{u}) - pI).\boldsymbol{\nu} &= 0 \ \text{ on } ]0,T[\times\Sigma_N && \text{(9i)}\\
\phi(0) &= \phi_0 \ \text{ in } \Lambda && \text{(9j)}\\
\mathbf{u}(0) &= \mathbf{u}_0 \ \text{ in } \Lambda && \text{(9k)}
\end{aligned}$$

where $\Sigma_N = \{-L, L\}^{d-1}\times]-L, L[$ is associated to a Neumann-type boundary condition.

Notice that equation (9b) is written in $\Lambda\backslash\partial\Omega$, i.e. in $\Omega$ and its complementary $\Lambda\backslash\overline{\Omega}$. On $\partial\Omega$, the jump term in (9e) points out the balance with membrane strengths: indeed, the first normal term comes from the Canham-Helfrich bending energy. This energy being a purely geometrical quantity, it cannot give rise to a tangential strength: any tangential movement of points on a surface is only modifying their positions without affecting the shape of the surface and its curvature energy. The second and third terms in (9e) involves the Lagrange multiplier $\lambda$, known as the surface tension, and defined on the membrane $\partial\Omega(t)$. The second term is normal and it is similar to the strengths of capillarities engendered by the surface tension when modelling of the dynamics of drops. The term $\nabla_s\lambda$ is tangential and its action is known as the Marangoni effect.

### *2.5. Dimensionless problem*

Let us put the problem in dimensionless form. The characteristic length $R_0$ of the vesicle is chosen equal to the radius of a sphere having the same surface as the vesicle $\partial\Omega$ in the tree dimensional case. In the two-dimensional case, it represents the radius of a circle having the same perimeter as $\partial\Omega$. The characteristic velocity $U = VR_0/L$ is chosen to be equal to the shear velocity at a distance $R_0$ from the center. The characteristic viscosity $\eta_0$ is chosen as the viscosity of the fluid at the exterior of the membrane.

Let us introduce the following four dimensionless numbers:

$$Re = \frac{\rho R_0 U}{\eta_0}, \quad Ca = \frac{\eta_0 R_0^2 U}{k}, \quad \alpha = \frac{R_0}{L} \ \text{ and } \ \beta = \frac{\eta_1}{\eta_0}$$

The Reynolds number $Re$, as usual, expresses the ratio of inertia effects with the viscous ones. The capillarity number $Ca$ compares the strength of the imposed flow $\eta_0 U/R_0$ to the bending resistance of the membrane $k/R_0^3$. The dimensionless

number $\alpha$ represents the confinement of the vesicle in the shear flow and $\beta$ is the viscosity ratio. The initial shape $\partial\Omega(0)$ is also characterized by a fifth dimensionless number: $\gamma$, the reduced area, already introduced in (2).

In the rest of the paper, only dimensionless quantities are used and, since there is no ambiguity, there are still denoted with the same notations as the original quantities. The dimensionless boundary condition writes:

$$\mathbf{u}_b(t,x) = \begin{cases} 1/\alpha & \text{when } x_d = \alpha \\ -1/\alpha & \text{when } x_d = -\alpha \end{cases}$$

A dimensionless viscosity function is also defined:

$$\eta_*(t,x) = \begin{cases} \beta & \text{when } x \in \Omega(t) \\ 1 & \text{otherwise} \end{cases}$$

The dimensionless problem writes:

*find $\phi$, $\mathbf{u}$, $p$ and $\lambda$ such that*

$$\begin{aligned}
\frac{\partial \phi}{\partial t} + \mathbf{u}.\nabla\phi &= 0 \ \text{ in } ]0,T[\times\Lambda && \text{(10a)}\\
Re\left(\frac{\partial \mathbf{u}}{\partial t} + \mathbf{u}.\nabla\mathbf{u}\right) - \mathbf{div}\left(2\eta_*\, D(\mathbf{u})\right) + \nabla p &= 0 \ \text{ in } ]0,T[\times(\Lambda\backslash\partial\Omega) && \text{(10b)}\\
\operatorname{div}\mathbf{u} &= 0 \ \text{ in } ]0,T[\times\Lambda && \text{(10c)}\\
[\mathbf{u}] &= 0 \ \text{ on } ]0,T[\times\partial\Omega && \text{(10d)}\\
-\frac{1}{Ca}\left\{\Delta_s H + H\left(\frac{H^2}{2} - 2K\right)\right\}\mathbf{n} & \\
+H\,\lambda\,\mathbf{n} - \nabla_s\lambda + \left[2\eta_*\, D(\mathbf{u}) - pI\right].\mathbf{n} &= 0 \ \text{ on } ]0,T[\times\partial\Omega && \text{(10e)}\\
\operatorname{div}_s\mathbf{u} &= 0 \ \text{ on } ]0,T[\times\partial\Omega && \text{(10f)}\\
\phi &= \phi_b \ \text{ on } ]0,T[\times\Sigma_- && \text{(10g)}\\
\mathbf{u} &= \mathbf{u}_b \ \text{ on } ]0,T[\times\Sigma_D && \text{(10h)}\\
(2\eta D(\mathbf{u}) - pI).\boldsymbol{\nu} &= 0 \ \text{ on } ]0,T[\times\Sigma_N && \text{(10i)}\\
\phi(0) &= \phi_0 \ \text{ in } \Lambda && \text{(10j)}\\
\mathbf{u}(0) &= \mathbf{u}_0 \ \text{ in } \Lambda && \text{(10k)}
\end{aligned}$$

where the normal and the curvature are expressed in term of the level set function: $\mathbf{n} = \nabla\phi/|\nabla\phi|$ and $H = \operatorname{div}_s\mathbf{n}$. Biophysical applications, as the prediction of vesicles behavior in small blood vessels, is our aim in this paper, and constitute a guideline for the choice of dimensionless parameters. Following Vitkova and al. [37] on vesicles under shear flow, we estimate the physical parameters:

$$\begin{array}{rcrlrcll}
R_0 & \approx & 5\times10^{-5} & \text{m}, & \rho & \approx & 10^3 & \text{kg/m}^3,\\
L & \approx & 10^{-3} & \text{m}, & \eta_0 & \in & \left[5\times10^{-4},\ 0.2\right] & kg.s^{-1}.m^{-1},\\
k & \approx & 10^{-19} & \text{J}. & & & &
\end{array}$$

The shear velocity at the wall $V$ is between $1.2\times10^{-2}$ and 0.12 m/s. These experimental values leads to consider the following dimensionless parameter ranges:

$$\begin{aligned}
Re &\in \left[1.5\times10^{-9},\ 1.5\times10^{-4}\right],\\
Ca &\in \left[3\times10^{3},\ 3\times10^{6}\right].
\end{aligned}$$

The vesicles are deflated with $\gamma$ between 0.92 and 0.99. While the experimental value of the confinement was $\alpha = 1/20$, the influence of this parameter is studied

by varying its value between 1/2 and 1/5 in the case of regular meshes and reaching 1/12 when using adaptive meshes methods, as presented in the next section. Finally, the viscosity ratio $\beta$ is varying around a critical value associated to a stability transition and are less than 20.

## 3. Numerical methods

### *3.1. Time discretization and the characteristic method*

For simplicity, the numerical methods are presented when $d = 2$: in that case the Gauss curvature is null: $K = 0$. Nevertheless, the methods extend to three-dimensional case, just inserting the computation of $K$ in the Canham-Helfrich force.

Let $0 = t^0 < t^1 < t^2 < ... < t^N = T$ be a subdivision of the time interval $[0, T]$ with a constant time step $\Delta t = t^{n+1} - t^n$, $n = 1, 2, ..., N$. At step $n = 0$, let $\phi^0 = \phi_0$ be the initial condition. For any $n \geq 1$, the unknowns $\phi^n$, $\mathbf{u}^n$, $p^n$ and $\lambda^n$ at time step $n$ are computed by induction, using values at previous time steps. The time discretization is performed by using the method of characteristics: for any $t > 0$ and $x \in \Lambda$, the characteristic curve $X(., x, ; t)$ passing at time $t$ through $x$ is defined by the following ordinary differential equation:

$$\left\{ \begin{array}{rcl} \dfrac{\partial X}{\partial t}(s, x; t) & = & \mathbf{u}\left(X(s, x; t), t\right), \quad s \in ]0, T[ \\ X(t, x; t) & = & x. \end{array} \right.$$

For any function $\varphi(t, x)$, the total derivative $D\varphi/Dt$ expresses:

$$\frac{D\varphi}{Dt}(t, x) = \left(\frac{\partial \varphi}{\partial t} + \mathbf{u}.\nabla\varphi\right)(t, x) = \frac{\partial}{\partial \tau}\left(\varphi\left(X(t, x; \tau), \tau\right)\right)|_{\tau=t}$$

Following Pironneau [31], this derivative is approximated by a first-order backward Euler scheme:

$$\frac{D\varphi}{Dt}(t^n, x) \approx \frac{\varphi(t^n, x) - \varphi(t^{n-1}, X_1^{n-1}(x))}{\Delta t}$$

where $X_1^{n-1}(x) = x - \Delta t\ \mathbf{u}^{n-1}(x)$ denotes the first-order forward Euler approximation of $X(t^{n-1}, x; t^n)$. The time-discretization of the transport equation (10a) leads to:

$$\phi^n = \phi^{n-1} \circ X_1^{n-1} \quad \text{in } \Lambda \tag{11}$$

Then, the vesicle shape at step $n$ is known:

$$\begin{array}{rcl} \partial\Omega^n & = & \{x \in \Lambda;\ \phi^n(x) = 0\} \\ \Omega^n & = & \{x \in \Lambda;\ \phi^n(x) < 0\} \end{array}$$

The dimensionless viscosity is also computed explicitly:

$$\eta_*^n = \left\{ \begin{array}{ll} \beta & \text{when } x \in \Omega^n \\ 1 & \text{otherwise} \end{array} \right.$$

Also, the normal $\mathbf{n}^n$ and the curvatures $H^n$ and $K^n$ are computed at this step, together with differential operators (5) on the surface $\partial\Omega^n$, and defined for any scalar function $f$ and any vector field $\mathbf{v}$ by:

$$\nabla_s^n f = (I - \mathbf{n}^n \otimes \mathbf{n}^n)\ \nabla f, \tag{12a}$$

$$\mathrm{div}_s^n\, \mathbf{v} = (I - \mathbf{n}^n \otimes \mathbf{n}^n) : \nabla \mathbf{v}, \tag{12b}$$

$$\Delta_s^n f = \mathrm{div}_s^n\ (\nabla_s^n f). \tag{12c}$$

For any $y \in \mathcal{C}^3([0,T])$, a Taylor expansion shows that:

$$\frac{\mathrm{d}y}{\mathrm{d}t}(t) = \frac{3y(t) - 4y(t-\Delta t) + y(t-2\Delta t)}{2\Delta t} + \mathcal{O}\left(\Delta t^2\right).$$

Based on this approximation and following [35, chap. 5], the time discretization of the inertia term is performed by using a second order combined characteristic and finite difference discretization method. Let us introduce the second-order characteristics:

$$\begin{aligned} \mathbf{u}^* &= 2\mathbf{u}^{n-1} - \mathbf{u}^{n-2} \\ X_2^{n-1}(x) &= x - \Delta t\ \mathbf{u}^*(x) \quad \text{a.e. } x \in \Lambda, \\ X_2^{n-2}(x) &= x - 2\Delta t\ \mathbf{u}^*(x) \quad \text{a.e. } x \in \Lambda. \end{aligned}$$

Notice that $\mathbf{u}^*$ represents a prediction by extrapolation of $\mathbf{u}$ at time $t_n$. The problem becomes:

*find* $\mathbf{u}^n$, $p^n$ *and* $\lambda^n$ *such that*

$$\begin{aligned} &\frac{Re}{2\Delta t}\left(3\mathbf{u}^n - 4\mathbf{u}^{n-1} o X_2^{n-1} + \mathbf{u}^{n-2} o X_2^{n-2}\right) \\ &\qquad -\mathbf{div}\left(2\eta_*^n D\left(\mathbf{u}^n\right)\right) + \nabla p^n = 0 \quad \text{in } \Lambda \backslash \partial\Omega^n, \quad (13a) \\ &\qquad \operatorname{div} \mathbf{u}^n = 0 \quad \text{in } \Lambda, \quad (13b) \\ &\qquad [\mathbf{u}^n] = 0 \quad \text{on } \partial\Omega^n, \quad (13c) \\ &-\frac{1}{Ca}\left(\Delta_s^n H^n + \frac{\left(H^n\right)^3}{2}\right)\mathbf{n}^n + H^n \lambda^n \mathbf{n}^n - \nabla_s^n \lambda^n \\ &\qquad + \left[2\eta_*^n D\left(\mathbf{u}^n\right) - p^n \mathbf{I}\right].\mathbf{n}^n = 0 \quad \text{on } \partial\Omega^n, \quad (13d) \\ &\qquad \operatorname{div}_s^n.\mathbf{u}^n = 0 \quad \text{on } \partial\Omega^n, \quad (13e) \\ &\qquad \mathbf{u}^n = \mathbf{u}_b \ \text{ on } \Sigma_D. \quad (13f) \end{aligned}$$

The second order induction on $\left(\mathbf{u}^n\right)_{n\geq 0}$ is bootstrapped by using the initial condition: $\mathbf{u}^{-1} = \mathbf{u}^0 = \mathbf{u}_0$, where $\mathbf{u}^{-1}$ stands here for a convenient notation. The previous scheme use two main steps. The first step (11) is an explicit computation involving the characteristics. The second step (13) is a linear generalized Stokes sub-system that involves a constraint on the boundary of the vesicle together with the usual incompressibility constraint. We point out that this scheme transforms a strongly nonlinear shape optimization problem into a succession explicit computations and linear subproblems. The next paragraph presents how such a linear subproblem is treated.

### *3.2. The generalized Stokes subproblem*

#### *3.2.1. Formulation*

Let us introduce the Canham-Helfrich force, that appears in the right-hand side of the generalized Stokes subproblem:

$$\mathbf{f}^n = \frac{1}{Ca}\left(\Delta_s^n H^n + \frac{\left(H^n\right)^3}{2}\right)\mathbf{n}^n. \quad (14)$$

where $\mathbf{n}^n = \nabla\phi^n/|\nabla\phi^n|$, $H^n = \mathrm{div}_s\,\mathbf{n}^n$ and $\phi^n$ is known at this step of the algorithm. The following bilinear forms are first introduced:

$$\begin{aligned}
m(\mathbf{u},\mathbf{v}) &= \int_\Lambda \mathbf{u}.\mathbf{v}\,\mathrm{d}x,\ \forall \mathbf{u},\mathbf{v} \in \left(L^2(\Lambda)\right)^2,\\
a^n(\mathbf{u},\mathbf{v}) &= \int_\Lambda 2\,\eta_*^n\, D(\mathbf{u}) : D(\mathbf{v})\,\mathrm{d}x,\ \forall \mathbf{u},\mathbf{v} \in \left(H^1(\Lambda)\right)^2,\\
b_1(\mathbf{v},q) &= -\int_\Lambda q\,\mathrm{div}\,\mathbf{v}\,\mathrm{d}x,\ \forall q \in L^2(\Lambda),\ \forall \mathbf{v} \in H(\mathrm{div},\Lambda),\\
b_2^n(\mathbf{v},\mu) &= -\int_{\partial\Omega^n} \mu\,\mathrm{div}_s^n\,\mathbf{v}\,\mathrm{d}s,\ \forall \mu \in H^{\frac{1}{2}}(\partial\Omega^n),\ \forall \mathbf{v} \in H(\mathrm{div}_s,\partial\Omega^n).
\end{aligned}$$

where $H(\mathrm{div},\Lambda) = \left\{\mathbf{s} \in \left(L^2(\Lambda)\right)^2;\ \mathrm{div}\,\mathbf{s} \in L^2(\Lambda)\right\}$ (see e.g. [15, 7]). The variational formulation of (13a)-(13f) writes:

($S$): *find* $\mathbf{u}^n \in \mathbb{V}(\mathbf{u}_b)$, $p^n \in L^2(\Lambda)$ *and* $\lambda^n \in H^{\frac{1}{2}}(\partial\Omega^n)$ *such that*

$$\begin{aligned}
&\frac{3Re}{2\Delta t} m\left(\mathbf{u}^n,\mathbf{v}\right) + a^n\left(\mathbf{u}^n,\mathbf{v}\right) + b_1\left(\mathbf{v},p^n\right) + b_2^n\left(\mathbf{v},\lambda^n\right)\\
&= m_s^n\left(\mathbf{f}^n,\mathbf{v}\right) + \frac{Re}{2\,\Delta t} m\left(4\mathbf{u}^{n-1}oX_2^{n-1} - \mathbf{u}^{n-2}oX_2^{n-2},\mathbf{v}\right), \qquad (15a)\\
&b_1\left(\mathbf{u}^n,q\right) = 0, \qquad (15b)\\
&b_2^n\left(\mathbf{u}^n,\mu\right) = 0, \qquad (15c)
\end{aligned}$$

for all $\mathbf{v} \in \mathbb{V}(0)$, $q \in L^2(\Lambda)$ and $\mu \in H^{\frac{1}{2}}(\partial\Omega^n)$.

*3.2.2. The Canham-Helfrich force*

Let us consider in details the Canham-Helfrich force, as defined in (14). The force involves fourth order derivatives of the level set function and a direct discretization approach would requires a high regularity finite element method, such as the Hermite one (see e.g. [6]) with $H^2$ and $C^1$ regularity. In order to use standard Lagrange finite element, with only $H^1$ and $C^0$ regularity, the fourth-order derivatives are treated here with a different approach, based on a duality argument.

Since $H^n = \mathrm{div}\,\mathbf{n}^n$ and $\mathbf{n}^n = \nabla\phi^n/|\nabla\phi^n|$, then $H^n$ involves the second order derivative of the level set function. Let us define the *skeleton* of $\Omega$ as the set of points that are equidistant to at least two distinct points of $\partial\Omega$ (see e.g. [3, p. 195]). In order to avoid division by $|\nabla\phi^n|$, that could vanish on the skeleton, two intermediate variables $\mathbf{r}^n = \nabla(|\nabla\phi^n|)$ and $G^n = H^n|\nabla\phi^n|$ are used. First, using a classical Green formula in $\Lambda$, $\mathbf{r}^n$ can be characterized as

$$\mathbf{r}^n \in H_0(\mathrm{div},\Lambda) \text{ and } \int_\Lambda \mathbf{r}^n.\mathbf{s}\,\mathrm{d}x = \int_\Lambda |\nabla\phi^n|\ \mathrm{div}\,\mathbf{s}\ \mathrm{d}x,\quad \forall \mathbf{s} \in H_0(\mathrm{div},\Lambda),$$

where $H_0(\mathrm{div},\Lambda) = \{\mathbf{s} \in H(\mathrm{div},\Lambda);\ \mathbf{s}.\boldsymbol{\nu} = 0\}$. Next, let us turn to $G^n$. A simple development leads to:

$$G^n|\nabla\phi^n| = -H^n\ |\nabla\phi^n|^2 = -\mathrm{div}\left(\frac{\nabla\phi^n}{|\nabla\phi^n|}\right)|\nabla\phi^n|^2 = \mathbf{r}^n.\nabla\phi^n - \Delta\phi^n|\nabla\phi^n|$$

The duality argument is used for the $\Delta\phi^n$ term at the right-hand side and $G^n$ is characterized by

$$G^n \in H^1(\Lambda) \text{ and } \int_\Lambda G^n\,\zeta\,|\nabla\phi^n|\,\mathrm{d}x = \int_\Lambda (\mathbf{r}^n.\nabla\phi^n)\,\zeta\,\mathrm{d}x + \int_\Lambda \nabla\phi^n.\nabla\zeta\,|\nabla\phi^n|\,\mathrm{d}x,\ \forall\zeta \in H^1(\Lambda).$$

Finally, $H^n$ is defined as the restriction to $\partial\Omega^n$ of $G^n/|\nabla\phi^n|$. Notice that this quantity is well defined since $|\nabla\phi^n|$ is not vanishing at the vicinity of $\partial\Omega^n$.

Let us consider the following Green formula on the closed surface $\Gamma^n = \partial\Omega^n$:

$$\int_{\Gamma^n} \Delta_s^n \xi \, \zeta \, \mathrm{d}s + \int_{\Gamma^n} \nabla_s^n \xi . \nabla_s^n \zeta \, \mathrm{d}s = 0, \ \forall \xi, \zeta \in H^1(\Gamma^n).$$

Then $Y^n = -\Delta_s H^n$ can be computed in a weak sense:

$$Y^n \in H^1(\partial\Omega^n) \ \text{ and } \ \int_{\partial\Omega^n} Y^n \ \zeta \, \mathrm{d}s = \int_{\partial\Omega^n} \nabla_s^n H^n . \nabla_s^n \zeta \, \mathrm{d}s, \ \forall \zeta \in H^1(\partial\Omega^n)$$

Let us summarize the procedure. The following additional bilinear forms are introduced:

$$\begin{aligned}
m_w^n(\phi, \psi) &= \int_\Lambda \varphi \, \psi \, |\nabla\phi^n| \, \mathrm{d}x, \ \forall \varphi, \psi \in L^2(\Lambda), \\
a_w^n(\phi, \psi) &= \int_\Lambda \nabla\varphi \, \nabla\psi \, |\nabla\phi^n| \, \mathrm{d}x, \ \forall \varphi, \psi \in H^1(\Lambda), \\
m_s^n(\xi, \zeta) &= \int_{\partial\Omega^n} \xi \ \zeta \, \mathrm{d}s, \ \forall \xi, \zeta \in L^2(\partial\Omega^n), \\
c^n(\xi, \zeta) &= \int_{\partial\Omega^n} \nabla_s^n \xi . \nabla_s^n \zeta \, \mathrm{d}s, \ \forall \xi, \zeta \in H^1(\partial\Omega^n).
\end{aligned}$$

Then, compute successively as:

$$\begin{aligned}
\mathbf{r}^n \in H_0(\mathrm{div}, \Lambda) \text{ and } m(\mathbf{r}^n, \mathrm{s}) &= -b_1(|\nabla\phi^n|, \mathbf{s}^n), \ \forall \mathbf{s} \in H_0(\mathrm{div}, \Lambda), \\
G^n \in H^1(\Lambda) \text{ and } m_w^n(G^n, \psi) &= a_w^n(\phi^n, \psi) + m(\mathbf{r}^n . \nabla\phi^n, \psi), \ \forall \psi \in H^1(\Lambda), \\
H^n &= \frac{G^n}{|\nabla\phi^n|} \ \text{ on } \ \partial\Omega^n, \\
Y^n \in H^1(\partial\Omega^n) \text{ and } m_s^n(Y^n, \zeta) &= c^n(H^n, \zeta), \ \forall \zeta \in H^1(\partial\Omega^n), \\
\mathbf{n}^n &= \frac{\nabla\phi^n}{|\nabla\phi^n|} \ \text{ on } \ \partial\Omega^n, \\
\mathbf{f}^n &= \frac{1}{Ca} \left( -Y^n + \frac{(H^n)^3}{2} \right) \mathbf{n}^n \ \text{ on } \ \partial\Omega^n.
\end{aligned}$$

*3.2.3. Extension and regularization*

The previous variational formulation involves integrals over the moving surface $\partial\Omega^n$: in order to avoid the explicit re-triangulation of the surface $\partial\Omega^n$ at each time step, integrals over $\partial\Omega^n$ are transformed into integrals over $\Lambda$. First, remarks that an integral over $\partial\Omega^n$ can be written as an integral over $\Lambda$ with the help of the level set function $\phi^n$ and the Dirac measure $\delta$:

$$\int_{\partial\Omega^n} \varphi \, \mathrm{d}s = \int_\Lambda \tilde{\varphi} \ |\nabla\phi^n| \ \delta(\phi^n) \, \mathrm{d}x$$

where $\tilde{\varphi}$ is an extension to $\Lambda$ of any function $\varphi$ defined in $\partial\Omega^n$. Also, the normal vector $\mathbf{n}^n$, defined over $\partial\Omega^n$, extends as $\nabla\phi^n/|\nabla\phi^n|$ to $\Lambda$. Since there is no ambiguity, this extension of the normal is still denoted by $\mathbf{n}^n$. Also, the notations for the extension to $\Lambda$ of the surface operators defined in (12) are still conserved. By this way, the Canham-Helfrich force, as expressed by (14), can be extended to $\Lambda$.

Nevertheless, the explicit management of Dirac measures is not an easy task in finite element methods. Thus, the previous extension is combined together with a

regularization procedure. Three sharp functions are here considered: the Heaviside function $\mathscr{H}(\phi^n)$, that acts as the indicator of $\Lambda\backslash\Omega^n$, the Dirac measure $\delta(\phi^n)$ that localizes the surface $\partial\Omega^n$, and the sign function $\mathrm{sgn}(\phi^n)$, that will be used in a forthcoming paragraph, for the redistancing of the level set function.

In order to avoid the triangulation of $\partial\Omega^n$, a banded region of width $2\varepsilon$ is introduced, for some $\varepsilon > 0$. The Heaviside $\mathscr{H}$, the Dirac $\delta$ and the sign functions are replaced respectively by $\mathscr{H}_\varepsilon$, $\delta_\varepsilon$ and $\mathrm{sgn}_\varepsilon$, defined for all $\phi \in \mathbb{R}$ by:

$$\begin{aligned}
\mathscr{H}_\varepsilon(\phi) &= \begin{cases} 0, & \text{when } \phi < -\varepsilon, \\ \dfrac{1}{2}\left(1 + \dfrac{\phi}{\varepsilon} + \dfrac{\sin\left(\dfrac{\pi\phi}{\varepsilon}\right)}{\pi}\right), & \text{when } |\phi| \le \varepsilon, \\ 1, & \text{otherwise,} \end{cases} \\
\delta_\varepsilon(\phi) &= \frac{\mathrm{d}\mathscr{H}_\varepsilon}{\mathrm{d}\phi}(\phi) = \begin{cases} \dfrac{1}{2\varepsilon}\left(1 + \cos\left(\dfrac{\pi\phi}{\varepsilon}\right)\right), & \text{if } |\phi| \le \varepsilon \\ 0, & \text{otherwise} \end{cases} \\
\mathrm{sgn}_\varepsilon(\phi) &= 2\mathscr{H}_\varepsilon(\phi) - 1
\end{aligned}$$

The sharp viscosity is also replaced by a smooth one:

$$\eta^n_{*,\varepsilon} = \beta + (1-\beta)\mathscr{H}_\varepsilon\left(\phi^n\right)$$

The previous bilinear forms admits a regularized counterpart:

$$\begin{aligned}
a^n_\varepsilon(\mathbf{u},\mathbf{v}) &= \int_\Lambda 2\,\eta^n_{*,\varepsilon}\, D(\mathbf{u}) : D(\mathbf{v})\,\mathrm{d}x,\ \forall \mathbf{u},\mathbf{v} \in \left(H^1(\Lambda)\right)^2, \\
m^n_{s,\varepsilon}(\mathbf{u},\mathbf{v}) &= \int_\Lambda \mathbf{u}.\mathbf{v}\,|\nabla\phi^n|\,\delta_\varepsilon\left(\phi^n\right)\,\mathrm{d}x,\ \forall \mathbf{u},\mathbf{v} \in \left(L^2(\Lambda)\right)^2, \\
b^n_{2,\varepsilon}(\mathbf{v},\mu) &= -\int_\Lambda \mu\,\mathrm{div}^n_s\,\mathbf{v}\,|\nabla\phi^n|\,\delta_\varepsilon\left(\phi^n\right)\,\mathrm{d}x,\ \forall \mu \in L^2(\Lambda),\ \forall \mathbf{v} \in \left(H^1(\Lambda)\right)^2, \\
c^n_\varepsilon(\xi,\zeta) &= \int_\Lambda \nabla^n_s\xi.\nabla^n_s\zeta\,|\nabla\phi^n|\,\delta_\varepsilon\left(\phi^n\right)\,\mathrm{d}x,\ \forall \xi,\zeta \in H^1(\Lambda)
\end{aligned}$$

The computation of the curvature $H^n$ is unchanged while the Canham-Helfrich force becomes: find $Y^n_\varepsilon \in H^1(\Lambda)$ such that

$$m_{s,\varepsilon}(Y^n_\varepsilon,\zeta) = c_\varepsilon(H^n,\zeta),\ \forall \zeta \in H^1(\Lambda).$$

Then, compute the extension to $\Lambda$ of the force:

$$\mathbf{f}^n_\varepsilon = \frac{1}{Ca}\left(-Y^n_\varepsilon + \frac{\left(H^n\right)^3}{2}\right)\mathbf{n}^n \ \text{ in } \Lambda.$$

Problem (15) admits a regularized variant:

$(S)_\varepsilon$: *find* $\mathbf{u}^n_\varepsilon \in \mathbb{V}(\mathbf{u}_b)$, $p^n_\varepsilon \in L^2(\Lambda)$ *and* $\lambda^n_\varepsilon \in L^2(\Lambda)$ *such that*

$$\begin{aligned}
&\frac{3Re}{2\Delta t} m\left(\mathbf{u}^n_\varepsilon,\mathbf{v}\right) + a^n_\varepsilon\left(\mathbf{u}^n_\varepsilon,\mathbf{v}\right) + b_1\left(\mathbf{v},p^n_\varepsilon\right) + b^n_{2,\varepsilon}\left(\mathbf{v},\lambda^n_\varepsilon\right) \\
&= m^n_{s,\varepsilon}\left(\mathbf{f}^n_\varepsilon,\mathbf{v}\right) + \frac{Re}{2\,\Delta t} m\left(4\mathbf{u}^n_\varepsilon o X^n_2 - \mathbf{u}^{n-1}_\varepsilon o X^{n-1}_2, \mathbf{v}\right), \qquad (16a) \\
&b_1\left(\mathbf{u}^n_\varepsilon, q\right) = 0, \qquad (16b) \\
&b^n_{2,\varepsilon}\left(\mathbf{u}^n_\varepsilon,\mu\right) = 0, \qquad (16c)
\end{aligned}$$

for all $\mathbf{v} \in \mathbb{V}(0)$, $q \in L^2(\Lambda)$ and $\mu \in L^2(\Lambda)$. Notice that the surface tension $\lambda^n_\varepsilon$ is now extended to $\Lambda$. The regularization parameter $\varepsilon$ will be chosen as proportional to the the mesh size $h$, as presented in the next paragraph.

*3.2.4. Finite element discretization*

The Taylor-Hood finite element approximation (see e.g. [7]) for the Stokes problem is considered here for the velocity-pressure approximation of the generalized Stokes problem. Let $\mathscr{T}_h$ a finite element triangulation of $\Lambda$, where $h > 0$ stands for the largest element diameter [6]. The following finite dimensional spaces are introduced:

$$\begin{aligned} X_h &= \left\{ q \in C^0\left(\overline{\Lambda}\right),\ q_{|K} \in \mathbb{P}_1,\ \forall K \in \mathscr{T}_h \right\}, \\ \mathbf{S}_h &= \left\{ \mathbf{s} \in X_h^2,\ \mathbf{s}.\boldsymbol{\nu} = 0 \text{ on } \partial\Lambda \right\}, \\ \mathbb{X}_h &= \left\{ \mathbf{u} \in \left(C^0\left(\overline{\Lambda}\right)\right)^2,\ \mathbf{u}_{|K} \in (\mathbb{P}_2)^d,\ \forall K \in \mathscr{T}_h \right\}, \\ \mathbb{V}_h(\mathbf{u}_b) &= \mathbb{X}_h \cap \mathbb{V}(\mathbf{u}_b). \end{aligned}$$

Let us assume that $\phi_h^n \in X_h$ is an approximation of $\phi^n$ at the $n$-th time step. The computation of the discrete Canham-Helfrich force write:

$$\begin{aligned} \mathbf{r}_h^n \in S_h \text{ and } m(\mathbf{r}_h^n, \mathrm{s}) &= -b_1(|\nabla\phi_h^n|,\, \mathbf{s}^n),\ \forall \mathbf{s} \in S_h, \\ G_h^n \in X_h \text{ and } m_w^n(G_h^n, \psi) &= a_w^n(\phi_h^n, \psi) + m(\mathbf{r}_h^n.\nabla\phi_h^n, \psi),\ \forall \psi \in X_h, \\ H_h^n &= \frac{G_h^n}{|\nabla\phi_h^n|} \text{ in } \Lambda, \\ Y_h^n \in X_h \text{ and } m_{s,\varepsilon}(Y_h^n, \zeta) &= c_\varepsilon(H_h^n, \zeta),\ \forall \zeta \in X_h, \\ \mathbf{n}_h^n &= \frac{\nabla\phi_h^n}{|\nabla\phi_h^n|} \text{ in } \Lambda, \\ \mathbf{f}_h^n &= \frac{1}{Ca}\left(-Y_h^n + \frac{(H_h^n)^3}{2}\right)\mathbf{n}_h^n \text{ in } \Lambda. \end{aligned}$$

The discrete generalized Stokes problem writes:

$(S)_h$: *find* $\mathbf{u}_h^n \in \mathbb{V}_h(\mathbf{u}_b)$, $p_h^n \in X_h$ *and* $\lambda_h^n \in X_h$ *such that*

$$\begin{aligned} &\frac{3Re}{2\Delta t} m\left(\mathbf{u}_h^n, \mathbf{v}\right) + a_\varepsilon^n\left(\mathbf{u}_h^n, \mathbf{v}\right) + b_1\left(\mathbf{v}, p_h^n\right) + b_{2,\varepsilon}^n\left(\mathbf{v}, \lambda_h^n\right) \\ &= m_{s,\varepsilon}^n\left(\mathbf{f}_h^n, \mathbf{v}\right) + \frac{Re}{2\,\Delta t} m\left(4\mathbf{u}_h^{n-1} o X_2^{n-1} - \mathbf{u}_h^{n-2} o X_2^{n-2}, \mathbf{v}\right), \qquad (17a) \\ &b_1\left(\mathbf{u}_h^n, q\right) = 0, \qquad (17b) \\ &b_{2,\varepsilon}^n\left(\mathbf{u}_h^n, \mu\right) = 0. \qquad (17c) \end{aligned}$$

for all $\mathbf{v} \in \mathbb{V}_h(0)$, $q \in X_h$ and $\mu \in L_h$. The previous finite-dimensional linear system involves the following matrix structure:

$$\begin{pmatrix} A & B_1^T & B_2^T \\ B_1 & 0 & 0 \\ B_2 & 0 & 0 \end{pmatrix}$$

Such systems has been extensively studied and various efficient strategies are known (see e.g. [14]). In the present paper, this system is solved efficiently by the preconditioned conjugate gradient algorithm, as implemented in the Rheolef C++ library [35].

*3.3. The transport subproblem*

*3.3.1. Redistanciation*

Due to the inextensibility of the vesicle membrane and the fluid incompressibility, the level set function $\phi$, initially chosen to be a signed distance, remains also, for any

$t > 0$, a signed distance among the advection step, as shown in appendix Appendix B. Nevertheless, after time and space discretization, we experimented that the approximation $\phi_h$ is no more a signed distance after the discrete counterpart of the advection step. As a consequence, an auxiliary problem called the *redistancing problem* has to be solved in order to keep the function $\phi_h$ as a signed distance. The redistancing step was detailed by the authors in a separate paper [26] and we recall here briefly the main idea. For all $t \in ]0, T[$, an advection problem depending on a pseudo-time $\tau$ is introduced and we shall find its stationary solution. Let $\tilde{\phi}(t, .)$ be the known level set function at time $t$ that is no more a distance function. The redistancing problem writes:

$$\left\{ \begin{array}{rll} \dfrac{\partial \psi}{\partial \tau}(\tau, x; t) + \mathbf{v}.\nabla\psi & = \operatorname{sgn}\left(\tilde{\phi}\,(t, x)\right) + \lambda(\tau, x : t)\, g(\psi) & \text{a.e. } (\tau, x) \in ]0, +\infty[\times\Lambda, \\ \psi(0, x; t) & = \tilde{\phi}(x, t) & \text{a.e. } x \in \Lambda. \end{array} \right. \tag{18}$$

where the advection vector field is $\mathbf{v} = \operatorname{sgn}\left(\tilde{\phi}\right) \dfrac{\nabla\psi}{|\nabla\psi|}$ and $\operatorname{sgn}\left(\tilde{\phi}\right)$ denotes the sign function and is equal to $0, -1, +1$ respectively on $\partial\Omega(t)$, inside $\Omega(t)$ and outside $\Omega(t)$. We note also that $\lambda(\tau, x; t)$ is a Lagrange multiplier that enforces the constraint of constant volume locally at $x \in \Lambda$. We chose $g(\psi) = \delta(\psi)|\nabla\psi|$, the Lagrange multiplier has an explicit average value $\lambda_{\mathcal{V}}$ over an arbitrary *finite volume* $\mathcal{V} \subset \Lambda$:

$$\lambda_{\mathcal{V}}(\tau; t) \quad = \quad \left\{ \begin{array}{ll} \dfrac{\int_{\mathcal{V}} \delta(\psi)\, \left(\mathbf{v}.\nabla\psi - \operatorname{sgn}\left(\tilde{\phi}\right)\right)\, \psi x}{\int_{\mathcal{V}} \delta(\psi)\, g(\psi)\, \mathrm{d}x} & \text{when } \mathcal{V} \cap \partial\Omega(t) \neq \emptyset \\ \\ 0 & \text{otherwise} \end{array} \right. \tag{19}$$

The stationary solution satisfies $|\nabla\psi| = 1$ almost everywhere in $\Lambda$, consequently $\psi(\infty, .; t)$ is a signed distance and is taken as the new level set function $\phi(t, .)$ at time $t$. Let us notice that the solution $\psi$ of the redistancing problem (18) preserve the position of $\partial\Omega(t)$: for any $\tau > 0$, the zero level set of $\psi(\tau, .; t)$ is the same zero level set of $\phi(t, .)$. As a result the volume $\operatorname{meas}(\Omega(t))$ is also preserved, this point has great importance for numerous applications. However, after discretization by finite difference or finite element methods, this property is satisfied only approximately. Let us introduce the `redistance` operator defined by $\phi(t, .) = \texttt{redistancing}(\tilde{\phi}(t, .))$.

Let $\tilde{\phi}^n$ be the approximation of $\tilde{\phi}(t)$, at time $t^n$ and $\psi^m, \mathbf{v}^m$ be approximations of $\psi(\tau), \mathbf{v}(\tau)$ respectively at $\tau^m$. The time discretization is performed by using the method of characteristics and the total derivative $D\psi/Dt$ is approximated by a first-order backward Euler scheme as previously. The redistancing problem (18) is solved explicitly:

$$\psi^{m+1} = \left\{ \begin{array}{ll} \psi^m & \text{when } |\tilde{\phi}^n| < \varepsilon \\ \psi^m \circ X^m_{\mathbf{v}_\varepsilon} + \Delta\tau\ \operatorname{sgn}_\varepsilon(\tilde{\phi}^n) & \text{otherwise} \end{array} \right. \tag{20}$$

Here, the characteristic have subscripts $\mathbf{v}_\varepsilon$ in order to avoid confusion. Let $W_h$ be the space of piecewise constant functions on $\mathcal{T}_h$ and $\pi_h$ denotes the Lagrange interpolation in $Q_h$. Let $\psi^0_h = \tilde{\phi}^{n+1}_h$. At any step $m \geq 0$ of the redistancing algorithm, suppose $\psi^m_h \in Q_h$ being known, and let $\mathbf{g}^m_h \in Q^d_h$ be the approximation of $\nabla\psi^m_h \in W^d_h$ defined by the following linear system:

$$\int_\Lambda \mathbf{g}^m_h.\boldsymbol{w}_h\, \mathrm{d}x = \int_\Lambda \nabla\psi^m_h.\boldsymbol{w}_h\, \mathrm{d}x, \quad \forall \boldsymbol{w}_h \in Q^d_h$$

A mass lumping procedure is used for this linear system: the integrals involved in the computation of the coefficients of the matrix associated to the $L^2$ scalar product

are evaluated by using the trapeze quadrature formula. By this way, the matrix of the linear system is replaced by a diagonal one, and the computation of $\mathbf{g}_h^m$ becomes explicit. Then, let

$$\mathbf{v}_{\varepsilon,h}^m = \pi_h \left( \mathrm{sgn}_\varepsilon \left( \tilde{\phi}_h^{n+1} \right) \frac{\mathbf{g}_h^m}{|\mathbf{g}_h^m|} \right)$$

Finally, the discrete version of the redistancing algorithm writes also explicitly:

$$\psi_h^{m+1} = \begin{cases} \psi_h^m & \text{when } |\tilde{\phi}_h^n| < \varepsilon \\ \pi_h \left\{ \psi_h^m \circ X_{\mathbf{v}_\varepsilon}^m + \Delta\tau \ \mathrm{sgn}_\varepsilon(\tilde{\phi}_h^n)(1 - |\nabla \psi_h^m|) \right\} & \text{otherwise} \end{cases} \tag{21}$$

*3.3.2. Improvement of the area and perimeter conservations*

Let us summarize here the resolution of the problem:

**Algorithm** 1

- $n = 0$: Let $\partial\Omega(0)$ be the initial shape and $\phi_h^0$ be its associated signed distance function. Let $\mathbf{u}_h^0 = \mathbf{u}_h^{-1} \in \mathbb{V}(\mathbf{u}_b)$ be the initial velocity field.
- $n \geq 1$: Let $\phi_h^{n-1} \in Q_h$ and $\mathbf{u}_h^{n-1}$, $\mathbf{u}_h^{n-2} \in \mathbb{V}_h(\mathbf{u}_b)$ being known. Then

  step 1 : compute $\tilde{\phi}_h^n = \pi_h \left( \phi_h^{n-1} \circ X_1^{n-1} \right) \in Q_h$;

  step 2 : compute $\phi_h^n = \texttt{redistancing}(\tilde{\phi}_h^n)$;

  step 3 : compute $\mathbf{u}_h^n$, $p_h^n$ and $\lambda_h^n$ from (17).

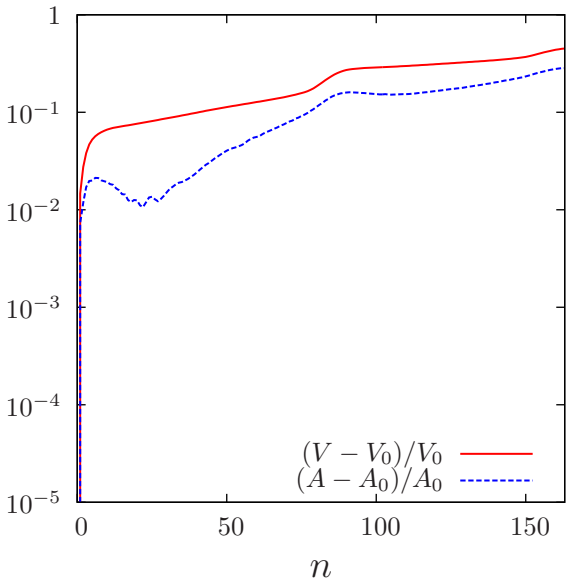


Figure 2: Without conservation improvement, the vesicle area and perimeter errors diverge: computations for $h = 5.3 \times 10^{-2}$, $\Delta t = 3 \times 10^{-2}$, $\tau = 0.81$ and $\varepsilon = 2.5\, h$.

In this section we present a numerical simulation to illustrate the features of the numerical method. We choose $Re = 10^{-3}$, $Ca = 10^3$, $\alpha = 1/10$, $\tau = 0.81$ and a viscosity rate $\beta = 50$. Fig. 2 plots the evolution of the relative error in vesicle area and perimeter. Observe that, after few iterations, the error becomes higher than 10% of the reference vesicle area and perimeter: this error completely changes the

vesicle, that evolves to a circular shape. The algorithm must be modified in order to improve the area and perimeter conservation. The problem of advection (4a) is substituted by the equivalent system:

$$\begin{aligned}
\frac{\partial \phi}{\partial t} + \left[\mathbf{u} + (p_* + \lambda_* f)\,\mathbf{n}\right].\nabla\phi &= 0 \quad \text{a.e } (t,x) \in ]0,+\infty[\times\Lambda\,, && (22)\\
\frac{\mathrm{d}}{\mathrm{d}t}\int_\Lambda (1-\mathscr{H}(\phi))\,\mathrm{d}x &= 0 \quad \forall t \in ]0,+\infty[\,, && (23)\\
\frac{\mathrm{d}}{\mathrm{d}t}\int_{\partial\Omega} \mathrm{d}s &= 0 \quad \forall t \in ]0,+\infty[\,, && (24)
\end{aligned}$$

where $p_*$ and $\lambda_*$ are two global Lagrange multipliers associated to two additional constraints for area and perimeter preservation. This system leads, after time discretization, to a modified and more robust scheme, with a modified advection field $\mathbf{u}_* = \mathbf{u} + (p_* + \lambda_* f)\,\mathbf{n}$. The variation of area $V(t)$ at time $t^n$ writes:

$$\frac{\mathrm{d}V}{\mathrm{d}t}(t^n) = \left[\frac{\mathrm{d}}{\mathrm{d}t}\int_\Lambda (1-\mathscr{H}(\phi))\,\mathrm{d}x\right]_{t=t^n} = \frac{V^n - V^{n-1}}{\Delta t} + \mathcal{O}(\Delta t)\,, \tag{25}$$

where $V^{n-1} = \int_{\Omega^{n-1}} \mathrm{d}x$ is known and we want to impose that $V^n = V_0$ the initial area, in order to avoid the previous area error accumulation. Conversely, the variation of the perimeter $A(t)$ at time $t^n$ expresses:

$$\frac{\mathrm{d}A}{\mathrm{d}t}(t^n) = \left[\frac{\mathrm{d}}{\mathrm{d}t}\int_{\partial\Omega} \mathrm{d}s\right]_{t=t^n} = \frac{A^n - A^{n-1}}{\Delta t} + \mathcal{O}(\Delta t)\,, \tag{26}$$

where $A^{n-1} = \int_{\partial\Omega^{n-1}} \mathrm{d}s$ is known and we want to impose that $A^n = A_0$ the initial perimeter. Combining (22) and (23), we obtain:

$$\frac{\mathrm{d}}{\mathrm{d}t}\int_\Lambda (1-\mathscr{H}(\phi))\,\mathrm{d}x = -\int_\Lambda \frac{\partial\phi}{\partial t}\delta(\phi)\,\mathrm{d}x = -\int_{\partial\Omega}\frac{1}{|\nabla\phi|}\frac{\partial\phi}{\partial t}\,\mathrm{d}s = \int_{\partial\Omega}\frac{1}{|\nabla\phi|}\mathbf{u}_*.\nabla\phi\,\mathrm{d}s\,. \tag{27}$$

Recall that, for any function $\varphi$ and vector field $\mathbf{v}$, the Reynolds formula on a surface $\partial\Omega$ writes:

$$\frac{\mathrm{d}}{\mathrm{d}t}\int_{\partial\Omega} f\,\mathrm{d}s = \int_{\partial\Omega}\frac{\mathrm{d}f}{\mathrm{d}t} + \nabla.(f\,\mathbf{u}) - f(\nabla\mathbf{u}.\mathbf{n}).\mathbf{n}\,\mathrm{d}s\,. \tag{28}$$

With $\varphi = 1$ and $\mathbf{v} = \mathbf{u}_*$, and using the Green formula (8), we get successively:

$$\frac{\mathrm{d}}{\mathrm{d}t}\int_{\partial\Omega}\mathrm{d}s = \int_{\partial\Omega}\mathrm{div}_s\,\mathbf{u}_*\,\mathrm{d}s = \int_{\partial\Omega} H\,\mathbf{u}_*.\mathbf{n}\,\mathrm{d}s. \tag{29}$$

At time $t^n$, replacing $\mathbf{u}_*^n$ by $\mathbf{u}^n + (p_*^n + \lambda_*^n f)\,\mathbf{n}^n$ in (25)-(26) and using (27)-(29), we obtain the following linear system with two unknowns $(p_*^n, \lambda_*^n) \in \mathbb{R}^2$:

$$\begin{aligned}
p^*\int_{\partial\Omega}\mathrm{d}s + \lambda^*\int_{\partial\Omega} f\,\mathrm{d}s &= \frac{V_0 - \int_{\Omega^n}\mathrm{d}x}{\Delta t} - \int_{\partial\Omega}\mathbf{u}.\mathbf{n}\,\mathrm{d}s\,,\\
p^*\int_{\partial\Omega} H\,ds + \lambda^*\int_{\partial\Omega} H\,f\,\mathrm{d}s &= \frac{A_0 - \int_{\partial\Omega^n}\mathrm{d}s}{\Delta t} - \int_{\partial\Omega} H\,\mathbf{u}.\mathbf{n}\,\mathrm{d}s\,.
\end{aligned}$$

Choosing $f$ a non-constant function ensure that this system is well-posed. In our simulations, we use $f(x_1,x_2) = 2x_1^2 + x_2^2$.

### *3.3.3. Improvement by mesh adaptation*

A way to adapt the mesh to the computation of a governing field is to equi-distribute its interpolation error, i.e. to make it constant over all triangles and in the directions

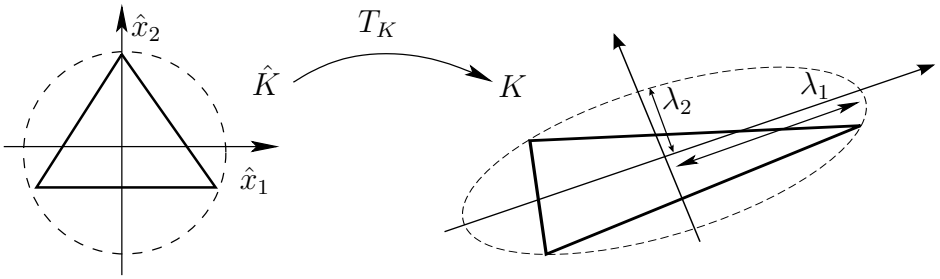


Figure 3: Transformation from the reference element $\hat{K}$ to any triangle $K$.

of maximal and minimal stretching and to adjust the maximal and minimal directions of stretching to others of maximal and minimal error. Our approach bases on the bidirectional anisotropic mesh generator `bamg` developed by F. Hecht [17] (see also [35, 19, 20]), together with the choice of a particular metric, specific to our time-dependent level set problem.

For any triangle $K$ of the mesh $\mathcal{T}_h$ at time $t$, let $T_K$ be the affine transformation which maps the reference triangle $\hat{K}$ into $K$ (see Fig. 3):

$$\begin{array}{rccl} T_K: & \hat{K} & \longrightarrow & K \\ & \hat{x} & \longmapsto & \mathbf{x} = T_K(\hat{\mathbf{x}}) = M_K \hat{\mathbf{x}} + \mathbf{t}_K \,. \end{array}$$

where $M_K$ is the Jacobian of $T_K$. Notice that $M_K$ is unsymmetric and invertible, otherwise $K$ would be flat. Thus, $M_K$ admits a singular value decomposition (for SVD, see [16, p. 69]): $M_K = R_K^T \Lambda_K P_K$, where $R_K$ and $P_K$ are orthogonal and where $\Lambda_K$ is diagonal with positive entries. The choice of the reference triangle $\hat{K}$ is not unique. It is common practice to choose as $\hat{K}$ the right triangle $\{(x_1, x_2), x_1 > 0, x_2 > O, x_1 + x_2 < 1\}$. For mesh generation and adaption purposes, an equilateral triangle, inscribed in the unit circle, is often preferred [13]. Since $\hat{x} = M_K^{-1}(x - t_K)$, the unit circle equation $\hat{x}^T \hat{x} = 1$ becomes:

$$1 = (x - t_K)^T M_K^{-T} M_K^{-1} (x - t_K) = (x - t_K)^T R_K^T \Lambda_K^{-2} R_K (x - t_K)$$

This is the equation of an ellipse containing $K$ (see Fig. 3).

Following [17], our choice of the metric is based on the hessian tensor of a specific governing field $\chi$, for which we aim at decreasing the interpolation error. The interpolation error in the direction $\mathbf{v} \in \mathbb{R}^2$ is given by:

$$e_{K,\mathbf{v}} = h_{K,\mathbf{v}}^2 \left\| \frac{\partial^2 \chi}{\partial \mathbf{v}^2} \right\| \quad \text{on } K,$$

where $h_{K,\mathbf{v}}$ denotes the length of $K$ in the direction $\mathbf{v}$ and $\dfrac{\partial^2 \chi}{\partial \mathbf{v}^2} = \mathbf{v}^T \nabla\nabla\chi \, \mathbf{v}$, and $\nabla\nabla\chi$ is the hessian matrix of $\chi$.

By adjusting the directional sizes $h_{K,\mathbf{v}}$ of $K$ for each eigenvector of the hessian matrix and each element $K$, the local directional interpolation errors can be equidistributed on the whole domain. An adaptation loop is required in order to assure the convergence of both the approximation of $\chi$ and its corresponding mesh. In order to adapt the mesh to the vesicle boundary $\partial\Omega^n$ at each time step $t_n$, the governing field $\chi = \delta_\varepsilon(\phi^n) + \delta_\varepsilon(\phi^{n-1})$ has been chosen for the adaptation loop. For an uniform mesh, the regularization parameter used for the computation of integrals over $\partial\Omega$ is chosen as proportional to the element size: $\varepsilon = 2h$. This choice is extended to a non-uniform mesh with a non-constant $\varepsilon(x)$, $x \in \Lambda$, that is proportional to an average

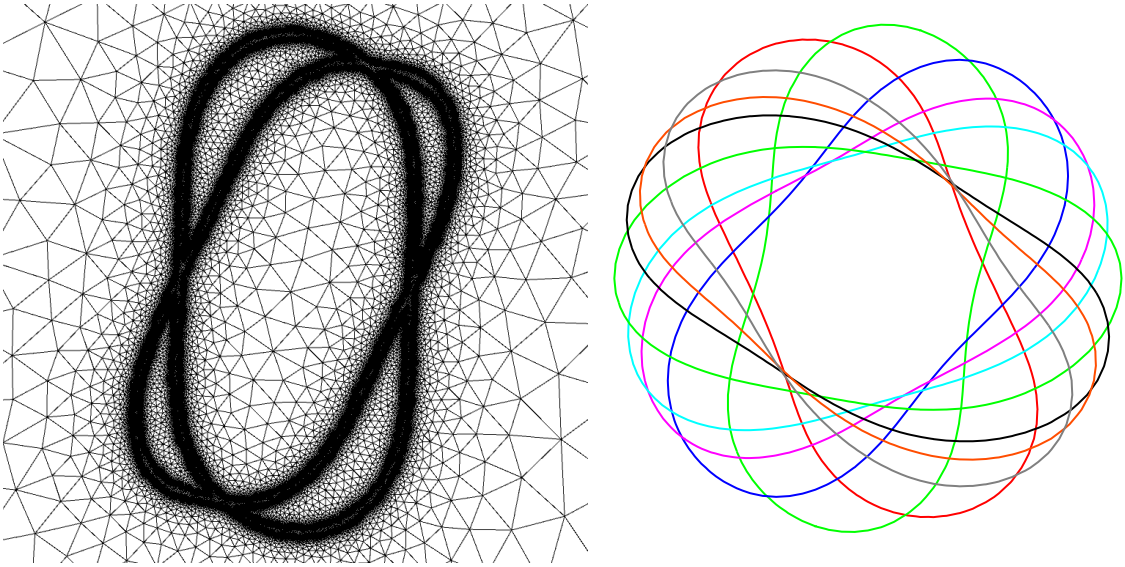

Figure 4: (left) Zoom on the adapted mesh ; (right) Vesicle tumbling under a linear shear flow for $Re = 10^{-3}$, $Ca = 10^4$, $\alpha = 1/4$, $\beta = 20$ and $\gamma = 0.89$. The shapes are shown for $t = kT_p/14$, $k \in \{1, 2, 3, 4, 5, 8, 11, 12, 13\}$, where $T_p = 10.3$ is the tumbling period.

value of the local mesh size: $\varepsilon(x) = 2\sqrt{2}\,\mathrm{meas(K)}^{\frac{1}{2}}$, for all $x \in K$. Fig. 4.a shows a zoom on the adapted mesh at the end of the adaptation loop, where both the contours of $\partial\Omega^{n-1}$ and $\partial\Omega^n$ are captured. Fig. 4.b represents the vesicle boundary evolution, as computed by the present auto-adaptive procedure.

## 4. Numerical results

### *4.1. Vesicles in the tumbling mode*

Simulations show, in accord with literature, that two flow regimes exist: a steady-state *tank-treading* regime where the vesicle assumes a steady-state shape and its inclination angle remains constant with time, while the fluid membrane treads as a tank and the internal fluid follows this rotation. The second regime is a periodic *tumbling* one, where the vesicle shape rotates. The transition between the two regimes for a vesicle of fixed reduced area $\gamma$ happens at a critical viscosity ratio between the inside and outside fluid, beyond which the vesicle tumbles. The small Reynolds number case is considered in this paragraph: this is a typical situation in microfluidic devices and the viscous forces are dominant over the inertial ones: the flow is almost laminar, and no turbulence can be observed, at least in the absence of vesicle. The following parameters are chosen: $Re = 10^{-4}$ , $Ca = 10^3$ , $\beta = 20$ and a vesicle with a reduced area $\gamma = 0.89$ The time step is $\Delta t = 2.5 \times 10^{-3}$. In their experimental tests, Vitkova and al. [37] use vesicles with a diameter $50\,\mu$m in a canal with a length 1 mm. This leads to a confinement equal to 1/20: notice that we use confinements between 1/2 and 1/5 when using an uniform mesh, and up to 1/12, in the case of an adapted mesh. The viscosity ratio $\beta$ is chosen such that the vesicle is in a tumbling mode.

First, let us check the improvement of the area and perimeter conservation, as introduced in the procedure of the previous section. Computations are first performed with $\alpha = 1/9$ and Fig. 5 plots the evolution of relative mass errors $(V - V_0)/V_0$ and $(A - A_0)/A_0$. Observe that, over a duration equivalent to 80 periods of tumbling,

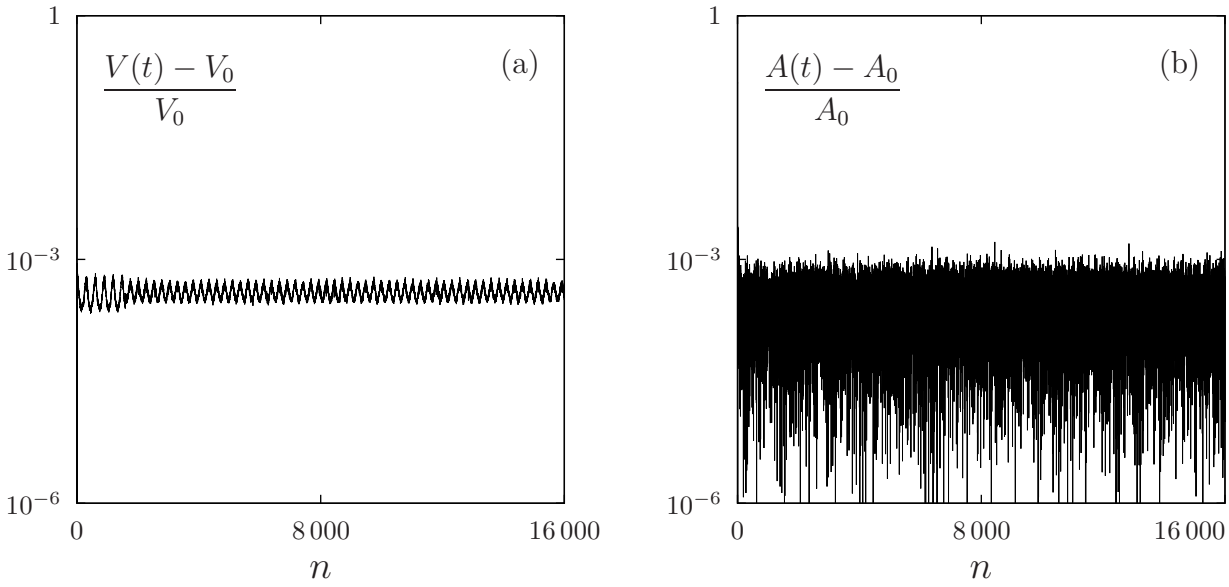


Figure 5: With conservation improvement, area and perimeter errors remains bounded: (a) the vesicle area error; (b) the vesicle perimeter error.

both the area and perimeter relative errors remains bounded by $10^{-3}$. The improvement of the conservation, based on Lagrange multipliers, is clearly shown by a comparison with the previous Fig. 2, where the errors diverge after the equivalent of two periods of the vesicle tumbling.

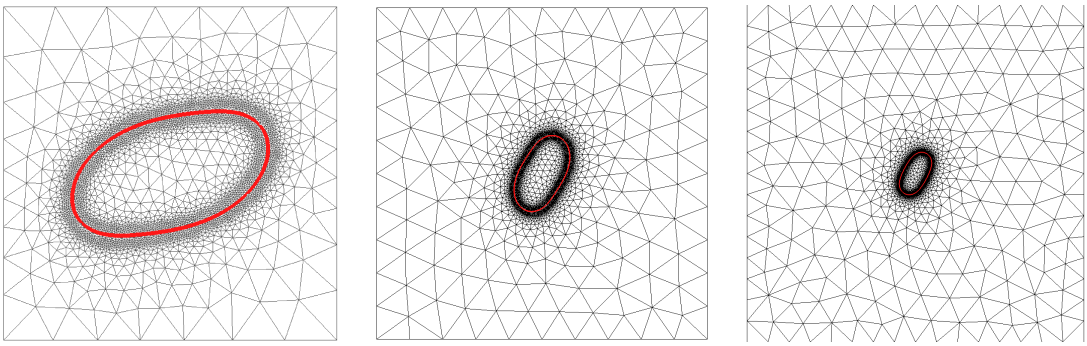

Figure 6: Adapted meshes used for the study of the effect of the confinement $\alpha$: from left to right: $\alpha = 1/2$, $1/5$ and $1/9$.

Let us now investigate the effect of the confinement $\alpha$ on the tumbling regime of the vesicle. Adapted meshes, that capture the vesicle boundary (in red) are shown in Fig. 6 for different confinements. Fig. 7 plots the evolution of the tumbling dimensionless period, denoted as $T_p$, versus $1/\alpha$. As it could be expected, these results show that when the confinement $\alpha$ decreases, the tumbling period becomes independent of $\alpha$. In the simulations presented in the rest of the paper, $\alpha = 1/4$ was chosen, since the solution it sufficiently independent of the confinement.

Let us denote by $\theta(t)$ the inclination angle measured counterclockwise from the positive $x_1$ semi-axis. The numerical computation of the inclination angle $\theta(t)$ for an arbitrary shape $\Omega(t)$ is reported in appendix Appendix C. The vesicle reaches a periodic regime after about 10 periods of tumbling: the inclination angle $\theta(t)$

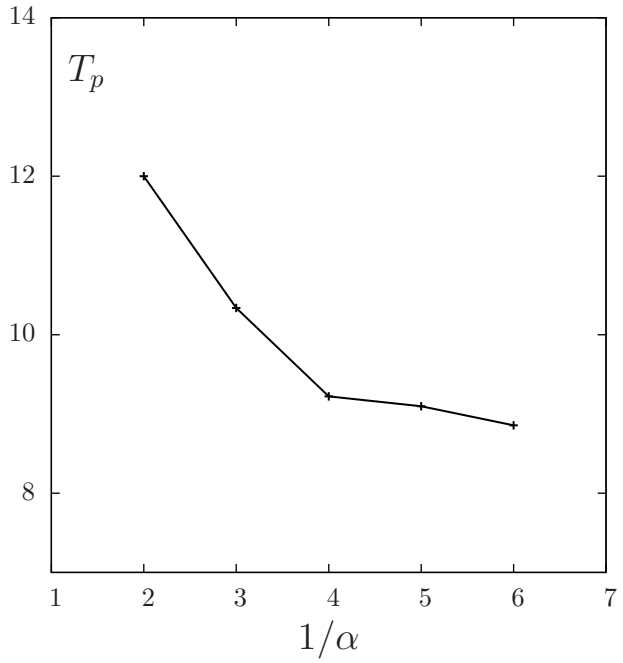


Figure 7: Tumbling regime: period $T_p$ *vs* $1/\alpha$ for $Re = 10^{-4}$, $Ca = 10^3$, $\beta = 20$ and $\gamma = 0.82$.

becomes periodic. Let us observe on Fig. 8 some Lissajous representations, suitable for periodic phenomenas. The solution is represented, during the $10^{th}$ period, where the periodic regime is well established. Fig. 8.a the angular velocity $\frac{d\theta}{dt}$ versus $\theta$: observe that the angular velocity is minimal when $\theta = 0$, i.e. when the vesicle is aligned with the horizontal axis, while its maximal when the vesicle is aligned vertically ($\theta = \pm\pi/2$). Fig. 8.b the evolution of the Canham-Helfrich energy versus $\theta$: this energy reaches a global maximum when the vesicle is roughly aligned horizontally and, conversely, reaches a minimum when its roughly aligned vertically. Here, there is a small phase shift: the extrema of the energy are slightly in advance with the corresponding extrema of the angular velocity.

In order to study analytically the dynamics of vesicles, a rough analytical model was proposed in 1982 by Keller and Skalak [22]. This model incorporates a quasi-inextensible membrane, but vesicles were treated as undeformable liquid ellipsoids. Nevertheless, this model was able to reproduce tumbling regime notably for reduced area $\gamma$ near 1 (i.e. quasi-spherical shapes), for which the distance to inextensibility is weak. Keller and Skalak [22] showed that the ellipsoid motion is described by:

$$\frac{\mathrm{d}\theta}{\mathrm{d}t} = -\frac{1}{2} + c(\gamma\,,\,\beta)cos(2\theta),$$

where $c(\gamma\,,\,\beta)$ is a coefficient depending on the aspect ratio $\gamma$ and the viscosity ratio $\beta$. Fig. 9 plots $\frac{\mathrm{d}\theta}{\mathrm{d}t}$ versus $cos(2\theta)$. Observe the good correspondence with the affine behavior, as predicted by the Keller and Skalak theory. A linear regression on the numerical simulation data leads to the slope coefficient $c = 0.33$.

Let us turn to the effect of the reduced area $\gamma$ on the period of tumbling $T_p$. We consider a vesicle with a viscosity ratio $\beta = 50$ in a shear flow with a Reynolds number $Re = 10^{-4}$ and a Capillarity number $Ca = 10^3$. Observe on Fig. 10 a quasi-linear dependence of $T_p$ upon $\gamma$.

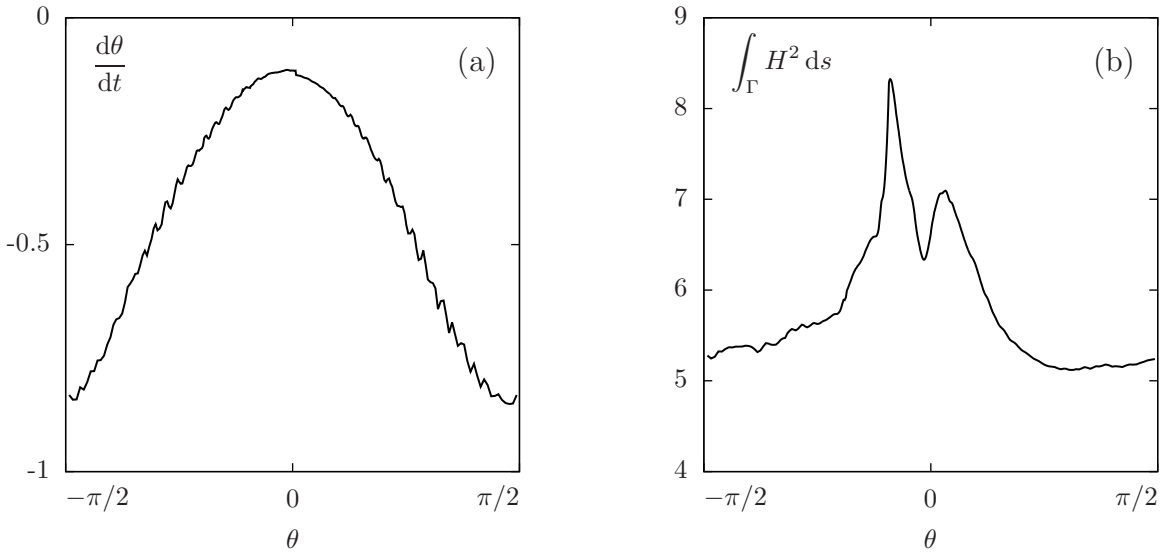


Figure 8: Tumbling regime: Lissajous curves: (a) the angular velocity $\frac{d\theta}{dt}$ *vs* $\theta$ and (b) the Canham-Helfrich energy *vs* $\theta$. ($Re = 10^{-4}$, $Ca = 10^3$, $\alpha = 1/4$, $\beta = 20$ and $\gamma = 0.82$).

### *4.2. The tank-treading regime*

When the viscosity contrast tends to the critical value of viscosity, a transition to the tank-treading regime occurs. When the viscosity contrast $\beta$ is small, the fluid inside the vesicle is highly deformed and rotated, and the vesicle adopts a stationary boundary $\partial\Omega$ ; its orientation $\theta(t)$ reaches rapidly a stationary value $\theta^*$ (see Fig. 11.a) Notice that the velocity is not vanishing along $\partial\Omega$: the membrane continue to tread like a tank and the internal fluid follows this rotation. Fig. 11.b plots the dependence of $\theta^*$ upon $\gamma$. Observe that $\theta^*$ increases versus $\gamma$.

Fig. 12 plots the streamlines and the velocity fields on the vesicle membrane. Remark that, when the stationary regime is reached, the velocity is tangential to the membrane.

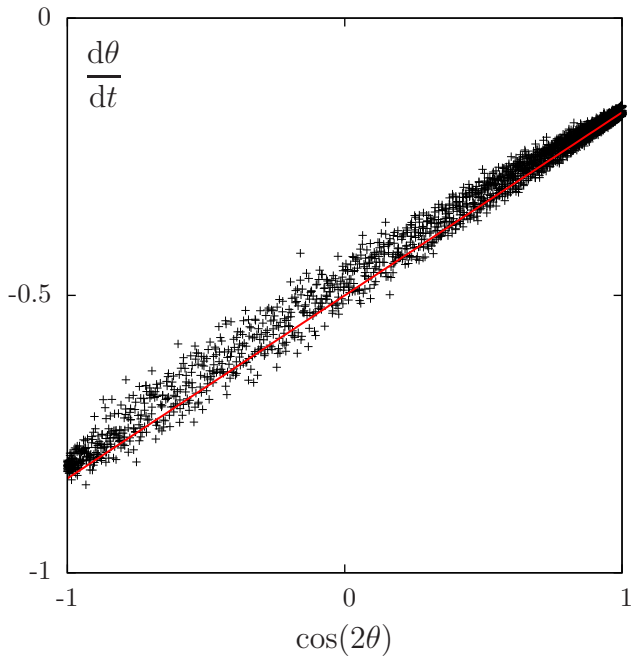


Figure 9: Tumbling regime: $\frac{d\theta}{dt}$ *vs* $cos(2\theta)$ for $Re = 10^{-4}$, $Ca = 10^4$, $\alpha = 1/9$, $\beta = 50$ and $\gamma = 0.84$. A linear regression leads to $\frac{d\theta}{dt} = 0.33\, cos(2\theta) - 0.5$, as indicated by the continuous line.

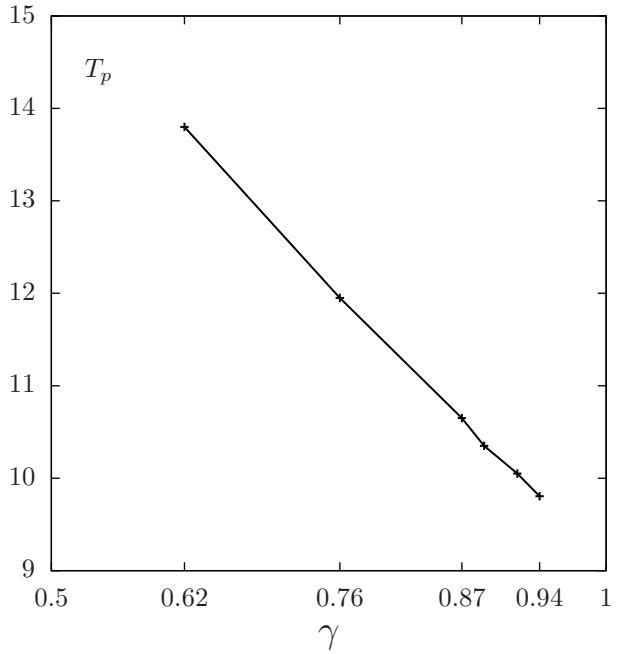


Figure 10: Tumbling regime: period $T_p$ *vs* the reduced area $\gamma$, for $Re = 10^{-4}$, $Ca = 10^3$, $\alpha = 1/4$ and $\beta = 50$.

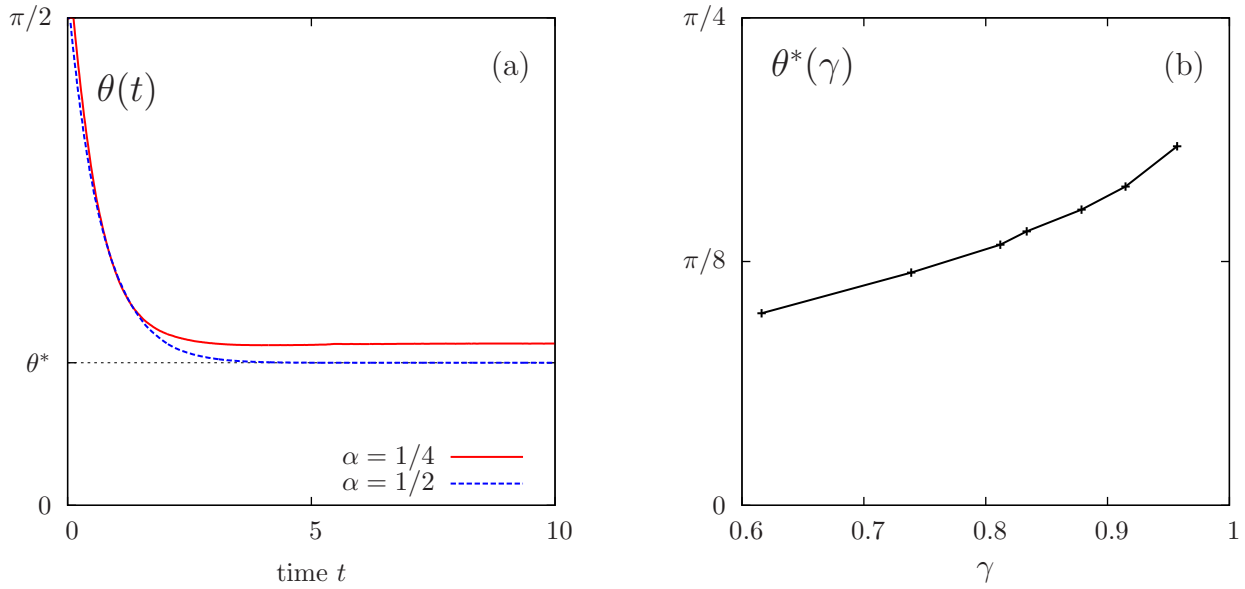


Figure 11: Tank-treading regime for $Re = 10^{-4}$, $Ca = 10^4$, $\beta = 1$ and $\gamma = 0.84$: (a) evolution of $\theta(t)$ for $\alpha = 1/2$ and $1/4$. (b) the stationary angle $\theta^* = \lim_{t\to+\infty} \theta(t)$ *vs* the reduced area $\gamma$ for $\alpha = 1/4$.

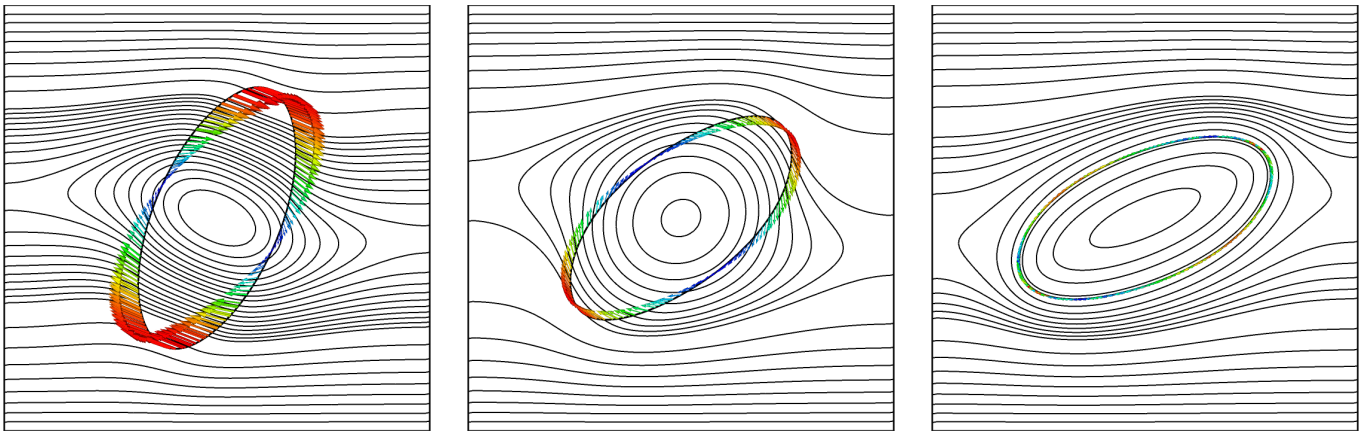

Figure 12: Tank-treading regime vs time for $Re = 10^{-4}$, $Ca = 10^4$, $\alpha = 1/2$, $\beta = 1$ and $\gamma = 0.84$: streamlines lines and velocity field on the vesicle membrane $\partial\Omega$. Figures are, from left to right, at $t = k\Delta t$, $k \in \{60, 120, 1000\}$ and $\Delta t = 2 \times 10^{-2}$.

*4.3. Effect of inertia*

An exhaustive study of the rheology of a vesicle in the presence of inertia has been carried out in this section. Although the basic behaviors had already been observed, the results shown in this part were nontrivial and not completely understood yet. For red blood cells in an blood vessel, the Reynolds number $Re$ is not always very small so the Stokes limit is not always available: $R_0$ is about $3 \times 10^{-6}$ m $\eta_0$ is about $10^{-3}$ Pa.s and $\rho$ is about $10^3$ kg.m$^{-3}$. For a mean velocity in the blood vessel about 1 m.s$^{-1}$, the Reynolds number $Re \approx 3$. In laboratory experiments, with experimental vesicles, $R_0$ is about $5 \times 10^{-5}$ m while we can supervise vesicles using rapid cameras that can reach a velocity of about 0.1 m.s$^{-1}$. In that case, the Reynolds numbers $Re \approx 5$. In both cases, the inertia effect can no more be neglected and the prediction of vesicle behaviors for these magnitude of the Reynolds number is of major importance. Moreover, we show in this paragraph, that inertia effects change dramatically the vesicle behavior for the simple shear flow.

Fig. 13 plots the evolution of the vesicle for $Re = 0.4$. Observe that the behavior, is dramatically different to the corresponding one for small Reynolds numbers, as shown previously on Fig. 4.b. Especially, deformations are more important when the inclination angle is close to $\pi/2$.

Above a critical value of the Reynolds number, the tumbling regime disappears: a new tank-treading regime occurs and the vesicle keeps a constant angle. Figs. 14.a and 14.b plot the angle $\theta(t)$ for $\gamma = 0.82$: observe that the period $T_p$ increases with $Re$ until a critical Reynolds number between 3.5 and 4. For $Re > 4$, the angle $\theta(t)$ becomes constant: the vesicle switch from a tumbling regime to a tumbling one. More developments on the effect of the inertia will appear in a forthcoming paper [27].

## 5. Conclusion

The new level method presented in this paper for the simulation of the vesicle dynamics exactly satisfies locally and at the discrete level both the inextensibility membrane condition and the volume conservation. We show that the proposed method, based on Lagrange multipliers, solves a lack of precision problem when dealing with the inextensibility constraints and the level set method. Moreover, an automatic adaptive method, used at each time step, enhance the prediction of the vesicle motion. With this procedure, we are able to accurately reproduce the change of regime, from tank-treading to tumbling, as observed when the viscosity ratio varies.

For the first time to our knowledge, we show the apparition of a new change of regime when the Reynolds number is below a critical value. Moreover, the critical Reynolds number of this order of magnitude for both red blood cells in arteries and vesicles used in laboratory experiments. In the future, new experiments on vesicle would be necessary to infirm or confirm your numerical predictions.

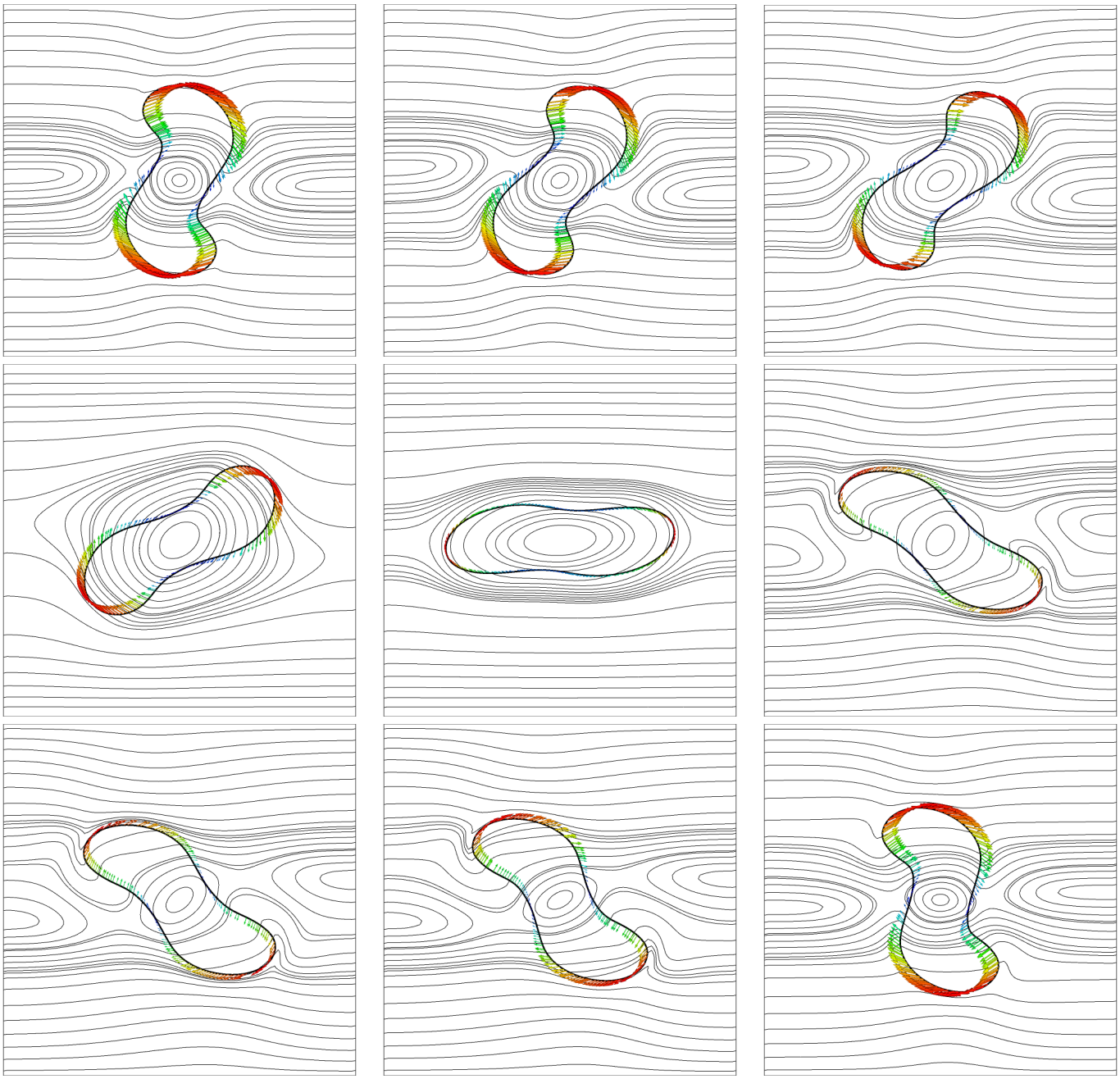

Figure 13: Inertia effects: streamlines lines and velocity field on the vesicle membrane for $Re = 0.4$, $Ca = 10^4$, $\alpha = 1/2$, $\beta = 10$ and $\gamma = 0.62$. Figure are shown, from left to right and top to bottom, at $t = kT_p/24$, $k \in \{2, 4, 6, 8, 13, 18, 20, 22, 24\}$, where $T_p = 29.1$ is the tumbling period.

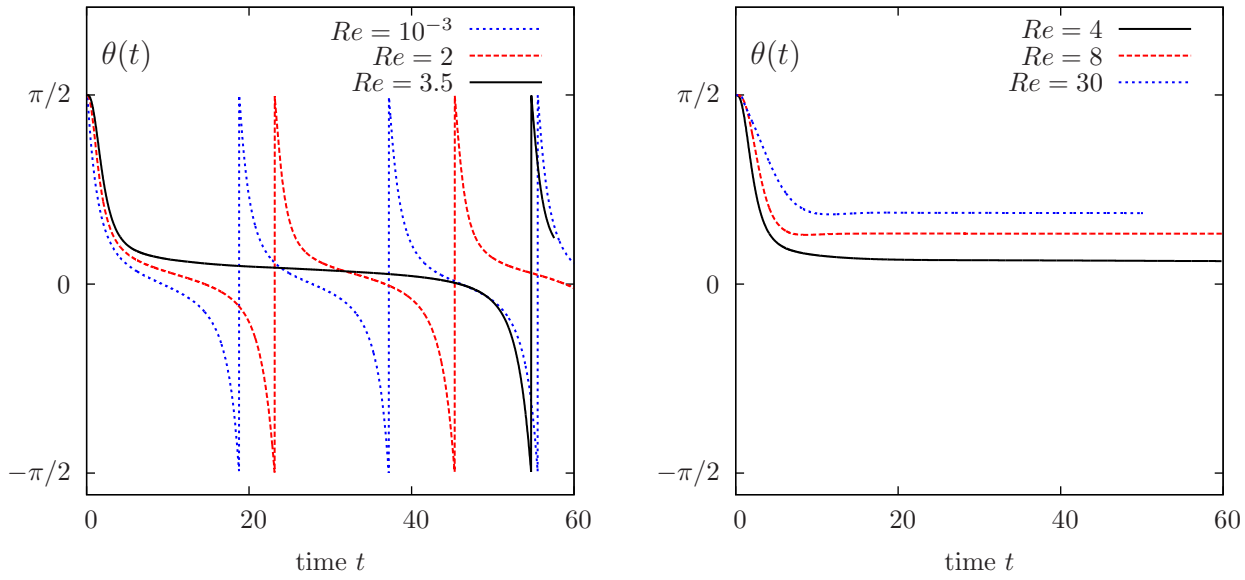


Figure 14: Inertia effect: influence of $Re$ on the vesicle inclination $\theta(t)$ for $Ca = 10^4$, $\alpha = 1/2$, $\beta = 10$ and $\gamma = 0.82$. (a) tumbling regime when $Re \leq 3/5$; (b) tank-treading regime when $Re \geq 4$.

[1] R. A. Adams and J. J. F. Fournier. *Sobolev spaces*. Elsevier, second edition, 2003.

[2] S. M. Allen and J. W. Cahn. A microscopic theory for antiphase boundary motion and its application to antiphase domain coarsening. *Acta Metal.*, 27:1085–1095, 1979.

[3] G. Aubert and P. Kornprobst. *Mathematical problems in image processing. Partial differential equations and the calculus of variations*. Springer, second edition, 2006.

[4] T. Biben, K. Kassner, and C. Misbah. Phase-field approach to three-dimensional vesicle dynamics. *Phys. Rev. E*, 72:041921, 2005.

[5] T. Biben and C. Misbah. Tumbling of vesicles under shear flow within an advected-field approach. *Phys. Rev. E*, 67:031908, 2003.

[6] S. C. Brenner and L. R. Scott. *The mathematical theory of finite element methods*. Springer, third edition, 2008.

[7] F. Brezzi and M. Fortin. *Mixed and hybrid finite element methods*. Springer, 1991.

[8] C. Bui, V. Lleras, and O. Pantz. Dynamics of red blood cells in 2d. *ESAIM Proc.*, 28:182–194, 2009.

[9] P. B. Canham. The minimum energy of bending as a possible explanation of the biconcave shape ogf the human red blood cell. *J. Theoret. Biol.*, 26:61–81, 1970.

[10] G.-H. Cottet, E. Maitre, and T. Milcent. Eulerian formulation and level-set models for incompressible fluid-structure interaction. *Math. Model. Numer. Anal.*, 42:471–492, 2008.

[11] Q. Du, C. Liu, R. Ryham, and X. Wang. Energetic variational approaches in modeling vesicle and fluid interactions. *Physica D*, 238:923–930, 2009.

[12] Q. Du, C. Liu, and X. Wang. A phase field approach in the numerical study of the elastic bending energy for vesicle membranes. *J. Comput. Phys.*, 198:450–468, 2004.

[13] L. Formaggia and S. Perotto. New anisotropic *a priori* error estimates. *Numer. Math.*, 89:641–667, 2001.

[14] M. Fortin and R. Glowinski. *Augmented Lagrangian methods*. Elsevier, 1983.

[15] V. Girault and P. A. Raviart. *Finite element methods for the Navier-Stokes equations. Theory and algorithms*. Springer, 1986.

[16] G. H. Golub and C. F. Van Loan. *Matrix computations*. The John Hopkins University Press, Baltimore, MD, USA, third edition, 1996.

[17] F. Hecht. *BAMG: bidimensional anisotropic mesh generator*, 2006. `http://www.rocq.inria.fr/gamma/cdrom/www/bamg/eng.htm`.

[18] W. Helfrich. Elastic properties of lipid bilayers: theory and possible experiments. *Z. Naturforsch*, 28(11):693–703, 1973.

[19] W. Huang. Metric tensors for anisotropic mesh generation. *J. Comput. Phys.*, 204:633–665, 2005.

[20] W. Huang and X. Li. An anisotropic mesh adaptation method for the finite element solution of variational problems. *Finite Elements in Analysis and Design*, 46:61–73, 2010.

[21] D. Jamet and C. Misbah. Toward a thermodynamically consistent picture of the phase-field model of vesicles: curvature energy. *Phys. Rev. E*, 78:031902, 2008.

[22] S. Keller and R. Skalak. Motion of a tank-treading ellipsoidal particle in a shear flow. *J. Fluid Mech.*, 120:27–47, 1982.

[23] Y. Kim and M.-C. Lai. Simulating the dynamics of inextensible vesicles by the penalty immersed boundary method. *J. Comput. Phys.*, 229(12):4840–4853, 2010.

[24] T. Krüger, F. Varnik, and D. Raabe. Efficient and accurate simulations of deformable particles immersed in a fluid using a combined immersed boundary lattice Boltzmann finite element method. *Comput. Math. Appl.*, 61(12):3485–3505, 2011.

[25] A. Laadhari, C. Misbah, and P. Saramito. On the equilibrium equation for a generalized biological membrane energy by using a shape optimization approach. *Phys. D*, 239:1568–1572, 2010.

[26] A. Laadhari, P. Saramito, and C. Misbah. Improving the mass conservation of the level set method. *C. R. Math*, 348:535–540, 2010.

[27] A. Laadhari, P. Saramito, and C. Misbah. Vesicle tumbling inhibited by inertia. *submitted*, 2011. `http://hal.archives-ouvertes.fr/hal-00604401`.

[28] E. Maitre, T. Milcent, G.-H. Cottet, A. Raoult, and Y. Usson. Applications of level set methods in computational biophysics. *Math. Comput. Model.*, 49(11–12):2161–2169, 2009.

[29] S. Osher and J. A. Sethian. Front propaging with curvature-dependent speed: agorithms based on Hamilton-Jacobi formulations. *J. Comput. Phys.*, 79(12), 1988.

[30] Z.-C. Ou-Yang and W. Helfrich. Bending energy of vesicle membranes: general expressions for the first, second and third variation of the shape energy and applications to spheres and cylinders. *Phys. Rev. A*, 39(10):5280–5288, 1989.

[31] O. Pironneau. On the transport-diffusion algorithm and its applications to the Navier-Stokes equations. *Numerische Mathematik*, 38(3):309–332, 1982.

[32] C. Pozrikidis. Numerical simulation of the flow-induced deformation of red blood cells. *Annals of Biomedical Engineering*, 31:1194–1205, 2003.

[33] A. Rahimian, S. K. Veerapaneni, and G. Biros. Dynamic simulation of locally inextensible vesicles suspended in an arbitrary two-dimensional domain, a boundary integral method. *J. Comput. Phys.*, 229(18):6466–6484, 2010.

[34] S. A. Safran. *Statistical thermodynamics of surfaces, interfaces and membranes.* Frontier in physics, vol. 90. Addison-Wesley, Reading, USA, 1994.

[35] P. Saramito. *Efficient C++ finite element computing with Rheolef.* CNRS and LJK, 2011. `http://www-ljk.imag.fr/membres/Pierre.Saramito/rheolef/rheolef.pdf`.

[36] U. Seifert. Configurations of fluid membranes and vesicles. *Adv. Phys*, 46:13–137, 1997.

[37] V. Vitkova, G.Coupier, M.-A. Mader, B. Kaoui, C. Misbah, and T. Podgorski. Tumbling of viscous vesicles in a linear shear field near a wall. *Journal of optoelectronics and advanced materials*, 11:1218–1221, 2009.

[38] P. M. Vlahovska, T. Podgorski, and C. Misbah. Vesicles and red blood cells in flow: from individual dynamics to rheology. *C. R. Physique*, 10:775–789, 2009.

## Appendix A. Remark on the spontaneous curvature

Let denote by $V_0$ the area and by $A_0$ the perimeter of the vesicle $\Omega$. Using as a characteristic length the radius $R_0$ of the circle having the same perimeter as $\partial\Omega$, the relation between the Lagrangian $\mathscr{L}$ and its dimensionless counterpart $\widetilde{\mathscr{L}}$ writes:

$$\widetilde{\mathscr{L}}(\widetilde{\Omega};\widetilde{\lambda},\widetilde{p}) = \frac{2R_0}{k_c}\,\mathscr{L}(\Omega;\lambda,p) = \int_{\partial\widetilde{\Omega}} \widetilde{H}^2\,\mathrm{d}\widetilde{s} + \widetilde{\lambda}\left(\int_{\partial\widetilde{\Omega}} \mathrm{d}\widetilde{s} - \widetilde{A}_0\right) + \widetilde{p}\left(\int_{\widetilde{\Omega}} \mathrm{d}\widetilde{x} - \widetilde{V}_0\right).$$

where $\widetilde{\lambda} = \dfrac{2}{k_c}\,\lambda R_0^2$ and $\widetilde{p} = \dfrac{2}{k_c}\,pR_0^3$. denote the dimensionless Lagrange multipliers. Recall that the reduced area $\gamma = \dfrac{V_0}{\pi} \times \left(\dfrac{2\pi}{A_0}\right)^2 = \dfrac{V_0}{\pi R_0^2}$. Then, for the dimensionless problem, the volume and area express $\widetilde{V}_0 = \dfrac{V_0}{R_0^2} = \pi\,\gamma$ and $\widetilde{A}_0 = \dfrac{A_0}{R_0} = 2\pi$. As a consequence, the reduced area $\gamma$ is the unique dimensionless number of this problem, that characterizes the stationary shape of the vesicle: others parameters, such as $k_c$, has no effects.

Let us turn to the effect of the spontaneous curvature $H_0 \geq 0$: The Lagrangian writes:

$$\mathscr{L}(\Omega;\lambda,p) = \frac{k_c}{2}\int_{\partial\Omega}(H-H_0)^2\,\mathrm{d}s + \lambda\left(\int_{\partial\Omega}\mathrm{d}s - A_0\right) + p\left(\int_{\Omega}\mathrm{d}x - V_0\right). \quad \text{(A.1)}$$

From $(H-H_0)^2 = H^2 - 2HH_0 + H_0^2$, notice first that the last $H_0^2$ term is constant and thus, has no effects in the minimization problem. The only term that depend upon $H_0$ is the second one, involving $H_0\int_{\partial\Omega} H\,\mathrm{d}s$. Using the general shape derivative analysis framework [25] with $f(H) = H$, we get, for any vector field $\mathbf{u}$:

$$\frac{\partial}{\partial\Omega}\left(\int_{\partial\Omega} H\,\mathrm{d}s\right)(\Omega).(\mathbf{u}) = \int_{\partial\Omega} 2K\,\mathbf{u}.\mathbf{n}\,\mathrm{d}s. \quad \text{(A.2)}$$

where $K$ is the Gauss curvature of $\partial\Omega$. As $K = 0$ for two dimensional problems, the bidimensional vesicle equilibrium shape is independent of $H_0$ and depends only of the reduced area $\gamma$. The spontaneous curvature $H_0$ is only pertinent for three-dimensional problems.

## Appendix B. Remark on the redistanciation procedure

Let us consider the transport equation: $D_t\phi = \partial_t\phi + \mathbf{u}.\nabla\phi = 0$. Using the summation of repeated indices convention, we get: $\partial_i\phi\;\partial_i\partial_t\phi + \partial_i\phi\;\partial_i\left(u_j\partial_j\phi\right) = 0$ that writes also equivalently: $(1/2)\;\partial_t\left(|\nabla\phi|^2\right) + |\nabla\phi|^2(\mathbf{n}\otimes\mathbf{n}) : \mathbf{u} + \partial_i\phi.\partial_i\left(u_j\partial_j\phi\right)$. Remark that:

$\partial_i\phi.\partial_i\left(u_j\partial_j\phi\right) = (1/2)\ u_j.\partial_j\left(\left(\partial_i\phi\right)^2\right) = (1/2)\ \mathbf{u}.\nabla\left(|\nabla\phi|^2\right) = |\nabla\phi|\mathbf{u}.\nabla(|\nabla\phi|)$.
Then, we obtain: $D_t(|\nabla\phi|) = |\nabla\phi|\ (\mathrm{div}_s\,\mathbf{u} - \mathrm{div}\,\mathbf{u})$. The density of the fluid is supposed to be constant, and the mass conservation leads to $\mathrm{div}\,\mathbf{u} = 0$. Moreover, in the context of vesicles, $\mathrm{div}_s\,\mathbf{u}$ since the membrane is supposed to be inextensible. Thus $D_t(|\nabla\phi|) = 0$. When $|\nabla\phi| = 1$ at $t = 0$, i.e. when $\phi$ is initially a distance function, this property is then preserved for all $t > 0$. When using the finite element approximation, we observe that this property is only approximately preserved, and thus, the redistancing procedure described in this paper is applied.

## Appendix C. Computation of the vesicle inclination

This appendix presents the computation of the angle $\theta$ of the shape $\Omega$. Let $(x_1, x_2)$ be the coordinate system for $\mathbb{R}^2$, containing the shape $\Omega$ and $\mathrm{d}x = \mathrm{d}x_1\mathrm{d}x_2$. The center of the vesicle is denoted by $(\bar{x}_1, \bar{x}_2)$, where $\bar{x}_1 = \left(\int_\Omega x_1\mathrm{d}x\right)/\mathrm{meas}(\Omega)$ and $\bar{x}_2 = \left(\int_\Omega x_2\mathrm{d}x\right)/\mathrm{meas}(\Omega)$. Let $I$ be the inertia matrix of the vesicle relative to the vertical axis in $(\bar{x}_1, \bar{x}_2)$:

$$I_O = \begin{pmatrix} \int_\Omega (x_1-\bar{x}_1)^2\,\mathrm{d}x & \int_\Omega (x_1-\bar{x}_1)(x_2-\bar{x}_1)\,\mathrm{d}x \\ \int_\Omega (x_1-\bar{x}_1)(x_2-\bar{x}_1)\,\mathrm{d}x & \int_\Omega (x_2-\bar{x}_1)^2\,\mathrm{d}x \end{pmatrix}.$$

This symmetric matrix has two real eigenvalues and orthogonal eigenvectors. The inclination angle $\theta$ is defined as the angle between the eigenvector associated to the largest eigenvalue, and the $x_1$ axis.